JEM Journal of Experimental Medicine

ARTICLE

Core 1–derived mucin-type O-glycosylation protects against spontaneous gastritis and gastric cancer

Fei Liu[1,2*], Jianxin Fu[2*], Kirk Bergstrom[2*], Xindi Shan[2], J. Michael McDaniel[2], Samuel McGee[2], Xia Bai[3,4], Weichang Chen[1], and Lijun Xia[2,3,5]

Core 1–derived mucin-type O-glycans (O-glycans) are a major component of gastric mucus with an unclear role. To address this, we generated mice lacking gastric epithelial O-glycans (GEC *C1galt1*$^{-/-}$). GEC *C1galt1*$^{-/-}$ mice exhibited spontaneous gastritis that progressed to adenocarcinoma with ∼80% penetrance by 1 yr. GEC *C1galt1*$^{-/-}$ gastric epithelium exhibited defective expression of a major mucus forming O-glycoprotein Muc5AC relative to WT controls, which was associated with impaired gastric acid homeostasis. Inflammation and tumorigenesis in GEC *C1galt1*$^{-/-}$ stomach were concurrent with activation of caspases 1 and 11 (Casp1/11)–dependent inflammasome. GEC *C1galt1*$^{-/-}$ mice genetically lacking Casp1/11 had reduced gastritis and gastric cancer progression. Notably, expression of Tn antigen, a truncated form of O-glycan, and CASP1 activation was associated with tumor progression in gastric cancer patients. These results reveal a critical role of O-glycosylation in gastric homeostasis and the protection of the gastric mucosa from Casp1-mediated gastric inflammation and cancer.

Introduction

Gastric cancer ranks fourth among the most common cancers and is the third leading cause of cancer-related death worldwide (Torre et al., 2015). The development of gastric cancer is a multistep process, including chronic nonatrophic gastritis, multifocal atrophic gastritis, intestinal metaplasia, dysplasia, and invasive carcinoma (Correa, 1992). However, how gastritis is initiated and transformed to gastric cancer remains unclear.

The gastric mucosa faces hostile luminal factors such as gastric acid, digestive enzymes, aggressive dietary factors, and microorganisms. Gastric tissues interface with this luminal environment through gastric gland–derived oligosaccharide-rich mucins. MUC5AC (mouse, Muc5AC) is the major type of gastric surface mucin, composed primarily of mucin-type O-linked oligosaccharides (O-glycans; Fu et al., 2008; Ju et al., 2008). O-glycans are initiated by the addition of GalNAc to serine or threonine (via the ppGalNAcT family of glycosyltransferases), forming the Tn antigen (GalNAcα-O-Ser/Thr), which is used to generate the core 1 structure (Galβ1,3GalNAcα-O-Ser/Thr) on which most complex and branched O-glycans are derived (Ju et al., 2008). The biosynthesis of core 1 is controlled by core 1 β1,3-galactosyltransferase (C1GalT1; also known as T-synthase; Ju et al., 2008).

Altered O-glycosylation of mucins has been linked to pathogenesis of gastritis and gastric cancer. For example, differences in ABO blood group antigen expression of glycoproteins modulate *Helicobacter pylori* binding to gastric mucosa in humans and mice (Borén et al., 1993; Ilver et al., 1998; Magalhães et al., 2009) and influence bacterial burdens and disease (Heneghan et al., 1998; Lindén et al., 2008). Truncated O-glycans have been associated with gastritis and gastric cancer (Balmaña et al., 2018; Mereiter et al., 2018). Exposure of the immature glycan Tn antigen is observed in biopsies of gastritis and gastric cancer patients independent of *H. pylori* status (Barresi et al., 2001; Persson et al., 2017). In vitro studies suggest O-glycan truncation itself may lead to cell-intrinsic defects that perturb epithelial homeostasis (Duarte et al., 2017; Radhakrishnan et al., 2014). However, the role of abnormal O-glycosylation in homeostasis of the gastric mucosa in vivo is unknown.

In this study, we report that mice with ablation of O-glycans in gastric epithelium develop spontaneous chronic gastritis and gastric cancer. O-glycan truncation down to Tn antigen led to dysregulated expression of the main gastric O-glycoproteins Muc5AC and Muc1, respectively, an impaired gastric mucus layer, and altered gastric acid homeostasis, respectively. These phenotypes were associated with chronic gastritis driven by caspase-1/caspase-11 (Casp1/11)–dependent inflammasomes in a microbiota-independent manner. Truncated O-glycans such as Tn antigen, along with inflammasome activation, were also

[1]Department of Gastroenterology, The First Affiliated Hospital of Soochow University, Suzhou, Jiangsu, China; [2]Cardiovascular Biology Research Program, Oklahoma Medical Research Foundation, Oklahoma City, OK; [3]Jiangsu Institute of Hematology, Collaborative Innovation Center of Hematology, Key Laboratory of Thrombosis and Hemostasis of Ministry of Health, The First Affiliated Hospital of Soochow University, Suzhou, Jiangsu, China; [4]State Key Laboratory of Radiation Medicine and Protection, Soochow University, Suzhou, China; [5]Department of Biochemistry and Molecular Biology, University of Oklahoma Health Sciences Center, Oklahoma City, OK.

*F. Liu, J. Fu, and K. Bergstrom contributed equally to this paper; Correspondence to: Lijun Xia: lijun-xia@omrf.org; Weichang Chen: weichangchen@126.com.

detected in gastric cancer biopsies of patients, suggesting clinical relevance of this pathway in the pathogenesis of this common disease.

Results

GEC *C1galt1*$^{-/-}$ mice develop spontaneous gastritis

Gastric epithelial cell (GEC) *C1galt1*$^{-/-}$ pups, which lack core 1 O-glycans in gastric epithelium (Fig. 1 A), were born healthy in Mendelian ratios. Immunohistochemical (IHC) staining revealed the exposure of Tn antigen, which marks the deleted core 1 O-glycans, in the *C1galt1*$^{-/-}$ gastric epithelium, but not in other cell types or in WT (*C1galt1*$^{f/f}$) littermate gastric epithelium (Fig. 1 B), confirming the specificity and efficiency of the deletion. In addition, this result suggests Tn was not masked by alternative glycosylation such as sialylation. Staining for Concanavalin A, a marker for N-glycosylated moieties, revealed no difference between WT and GEC *C1galt1*$^{-/-}$ mice (Fig. S1 A), supporting that *C1galt1* deletion did not hinder *N*-glycosylation in stomach tissues. Gross analysis of the stomach revealed thickening of the antrum, but not corpus, of the stomach of 8- or 16-wk-old GEC *C1galt1*$^{-/-}$ versus WT littermates (Fig. 1 C). Histology showed spontaneous gastritis characterized by gastric mucosal hyperplasia and increased immune cell infiltration in the antrum of GEC *C1galt1*$^{-/-}$ mice (Fig. 1, D–F), while the corpus was not affected (Fig. S1 B). The morphology of chief cells and parietal cells, which are two major cell types of the gastric corpus, were similar between WT and GEC *C1galt1*$^{-/-}$ mice, indicating that *C1galt1* deficiency did not influence the development of the stomach in mice (Fig. S1 B). Mucosal thickening and disease were observed as early as 2 wk of age in GEC *C1galt1*$^{-/-}$ mice (Fig. S1, C and D) and progressed over time (Fig. 1, E and F). Taken together, these data show loss of core 1–derived O-glycans in the gastric epithelium leads to severe spontaneous chronic gastritis in the stomach antrum.

GEC *C1galt1*$^{-/-}$ mice show spontaneous gastritis-associated cancer

Chronic gastritis promotes gastric cancer in humans. We therefore determined whether chronic gastritis leads to gastric cancer in GEC *C1galt1*$^{-/-}$ mice by letting mice age up to 18 mo. As early as 6 mo of age, dysplasia was observed in the gastric antrum of GEC *C1galt1*$^{-/-}$ mice, but not WT littermates (Fig. 2 A). At age 12–18 mo, overt tumors were observed in the same region (Figs. 2 A and S1 E). Similar to gastritis, these tumors were localized to the antrum but not present in the forestomach or corpus of the GEC *C1galt1*$^{-/-}$ stomach. Histological analysis of tumor epithelial cells showed loss of polarity, a high nuclear-to-cytoplasmic ratio, and extensive stratification (Figs. 2 A and S1 E), consistent with the phenotype of adenomas. At the ages of 6–12 mo and 12–18 mo, 78% and 95% of GEC *C1galt1*$^{-/-}$ mice, respectively, exhibited tumors that increased in size and frequency over time (Fig. 2, B and C). Adenocarcinoma was evident from the presence of invasive dysplastic glands within the submucosa in aged GEC *C1galt1*$^{-/-}$ mice, with an incidence of ∼60% versus WT littermates (Fig. 2, D and E; and Fig. S1 F). These results showed that loss of gastric epithelial core 1–derived O-glycans leads to the initiation and progression of spontaneous gastritis-associated gastric cancer in our model.

Mucosal inflammasomes promote gastritis in GEC *C1galt1*$^{-/-}$ mice

We next sought to elucidate the mechanism underlying spontaneous gastritis and gastric cancer in GEC *C1galt1*$^{-/-}$ mice. Casp1-dependent inflammasomes have been implicated in inflammation-associated cancer in the gastrointestinal tract (Hitzler et al., 2012; Yin et al., 2015; Bergstrom et al., 2016); therefore, we examined its relevance to gastric diseases in GEC *C1galt1*$^{-/-}$ mice. We found that Casp1 was activated beginning as early as 2 mo of age, as shown by Western blot for the active p10 subunit of Casp1 in GEC *C1galt1*$^{-/-}$ versus WT mice (Fig. 3, A and B). Consistent with inflammasome activation, we observed elevated secretion of Casp1 substrates IL1β and IL18 within supernatants derived from GEC *C1galt1*$^{-/-}$ versus WT antrum organ cultures (24 h) from 5- and 12-mo-old mice (Fig. 3 C). Immunostaining for Casp1 showed a strong signal in antral glands of WT and GEC *C1galt1*$^{-/-}$ mice, including within invasive carcinoma of 18-mo-old mice (Fig. 3 D). To determine a role for this pathway in our model, we crossed GEC *C1galt1*$^{-/-}$ mice with mice lacking both Casp1 and Casp11 (*Casp1*$^{-/-}$;*Casp4*^{del}), which do not signal through canonical and noncanonical inflammasomes (Bergstrom et al., 2016), to generate GEC *C1galt1*$^{-/-}$; *Casp1/11*$^{-/-}$ mice (TKO) mice (Fig. 3 E). At 4 mo of age, when chronic gastritis is established in GEC *C1galt1*$^{-/-}$ mice (Fig. 1), TKO mice showed reduced thickening of the antrum compared with GEC *C1galt1*$^{-/-}$ littermates (Fig. 3 F). Histology confirmed the reduced mucosal hyperplasia and disease of TKO mice versus GEC *C1galt1*$^{-/-}$ mice (Fig. 3, F and G). Staining of WT, GEC *C1galt1*$^{-/-}$, and TKO antrum tissues with anti-Casp1, showed the epithelial Casp1 signal in WT and GEC *C1galt1*$^{-/-}$ mice but was undetectable in TKO mice, confirming antibody specificity and knockout status (Fig. S2 A). The inflammation in GEC *C1galt1*$^{-/-}$ mice was characterized by a significant increase in infiltrating granulocytes (MPO^{+}) versus WT and TKO littermates, although TKO still showed modest MPO^{+} cell influx versus WT (Fig. 3, H and I). Consistent with increased inflammatory cell flux, the expression of prototypical inflammatory cytokines *il6*, *tnfa*, and the *cxcl1* chemokine and, to a lesser extent, *il17* were all significantly upregulated in GEC *C1galt1*$^{-/-}$ mice versus WT and TKO (Fig. 3 J). Collectively, these results indicate that gastric inflammasomes play a significant role in the development of spontaneous gastritis in GEC *C1galt1*$^{-/-}$ mice.

Gastric cancer in GEC *C1galt1*$^{-/-}$ mice is dependent upon mucosal inflammasomes

We next determined whether spontaneous gastritis-associated tumorigenesis was also dependent upon inflammasomes. As expected, most 12-mo-old GEC *C1galt1*$^{-/-}$ mice developed large overt tumor masses in the antrum while WT did not; however, TKO mice also showed evidence of tumorigenesis at this age, although tumor incidence and volume was reduced versus GEC *C1galt1*$^{-/-}$ littermates (Fig. 4, A–C). Consistent with this, a reduced incidence of carcinoma was observed in the stomach of TKO versus age-matched or littermate GEC *C1galt1*$^{-/-}$ mice

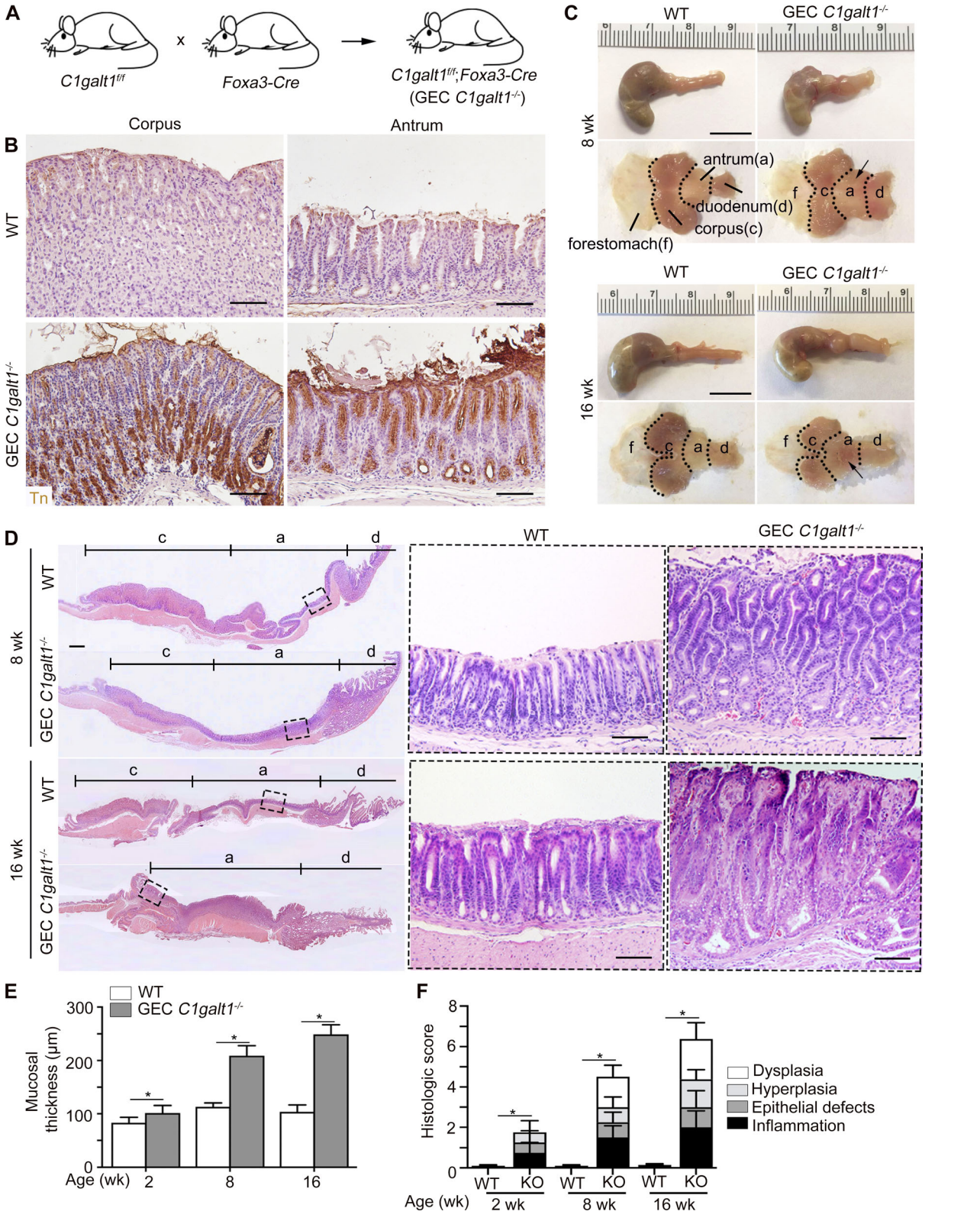

Figure 1. **GEC *C1galt1*$^{-/-}$ mice develop spontaneous gastritis. (A)** Model of generation GEC *C1galt1*$^{-/-}$ mice. **(B)** IHC staining of WT and GEC *C1galt1*$^{-/-}$ stomach sections with anti-Tn at 4 wk. Brown, positive staining. Scale bars, 50 µm. **(C)** Representative gross morphology of murine stomach with specific regions annotated as shown. Arrow points to a thickened, inflamed region of antrum. Scale bars, 1 cm. a, antrum; c, corpus; d, duodenum; f, forestomach. **(D)** Tiled H&E staining of stomach sections. Inset: Magnified boxed region in left image. Scale bars, 50 µm. **(E)** Quantitation of mucosal thickness of the gastric antrum mucosa. **(F)** Gastric histological score pooled from individual parameters shown. Results are means ± SD with four or five mice per group or time point. All data are representative of three independent experiments with at least four mice per group. *, $P < 0.05$.

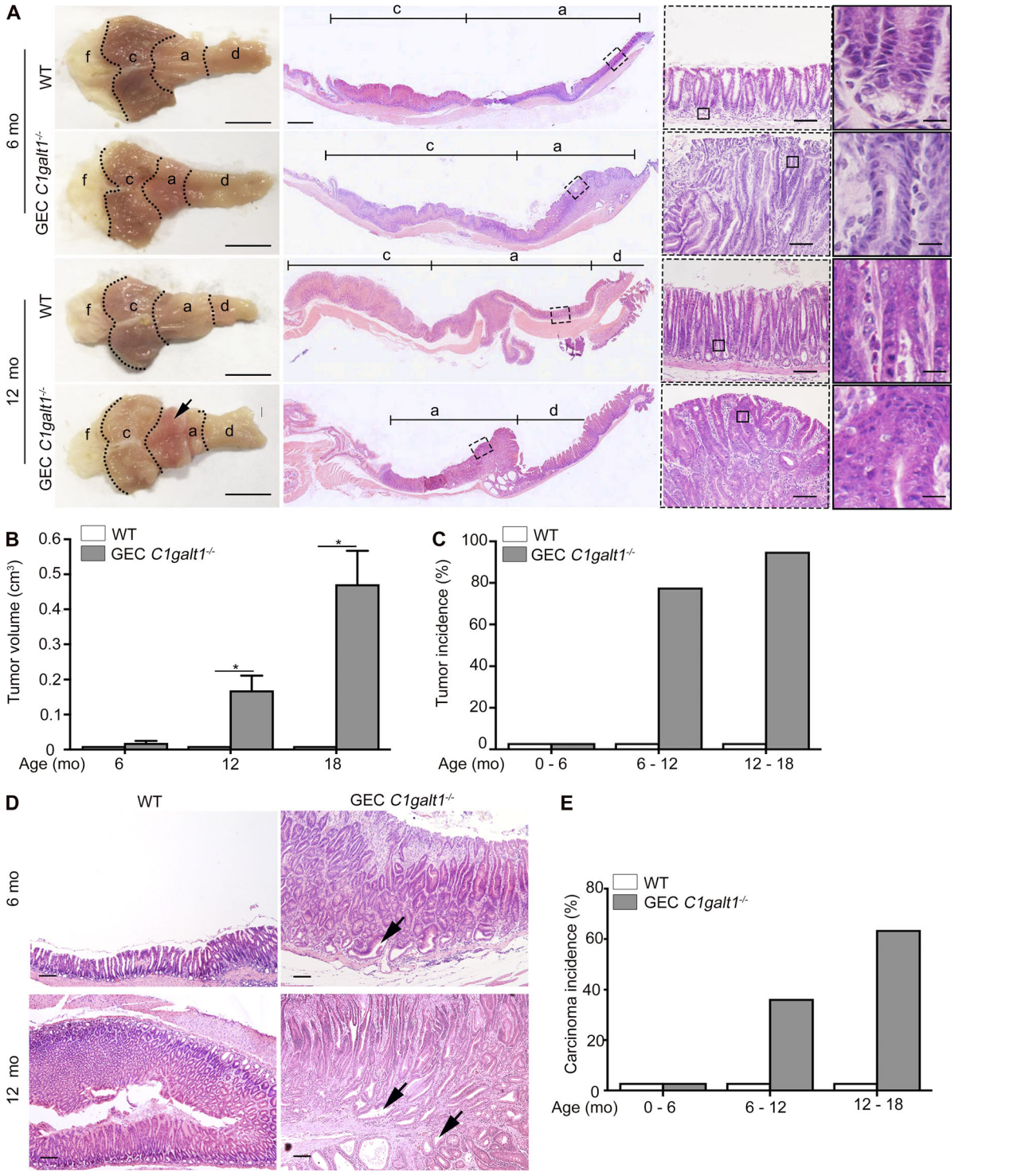

Figure 2. **GEC *C1galt1*$^{-/-}$ mice develop spontaneous gastric cancer. (A)** Gross morphology and H&E staining of murine stomach. Arrow points to a gastric tumor. Inset: Magnified images of boxed regions on left. Scale bars, 1 cm (gross morphology); 200 µm (tiling images); 50 µm (left inset); 12.5 µm (right inset). a, antrum; c, corpus; d, duodenum; f, forestomach. **(B)** Mean tumor volume (mean ± SD). **(C)** Tumor incidence (percentage of mice with tumors). **(D)** H&E staining of antrum. Arrows indicate carcinoma. Scale bars, 125 µm. **(E)** Incidence of gastric carcinoma. Data are representative of at least two independent experiments (mean ± SD; *n* = 8–10 mice/group for A, C, and D; *n* = 4–5 mice/group for B). *, P < 0.05.

(Fig. 4, A and D). In total, ∼50% of TKO mice at the age of 6–12 mo developed antrum tumors compared with 78% of GEC *C1galt1*$^{-/-}$ mice (Fig. 4, A and B). Between 12–18 mo, 95% of GEC *C1galt1*$^{-/-}$ mice developed tumors versus 67% of TKO mice (Fig. 4 B). Consistent with Casp1 activation at these time points, elevated IL1β and IL18 secretion were detected in tumor tissues from 18-mo-old GEC *C1galt1*$^{-/-}$ versus WT and TKO mice (Fig. 4 E). Ablation of the Casp1 signal was confirmed in the gastric

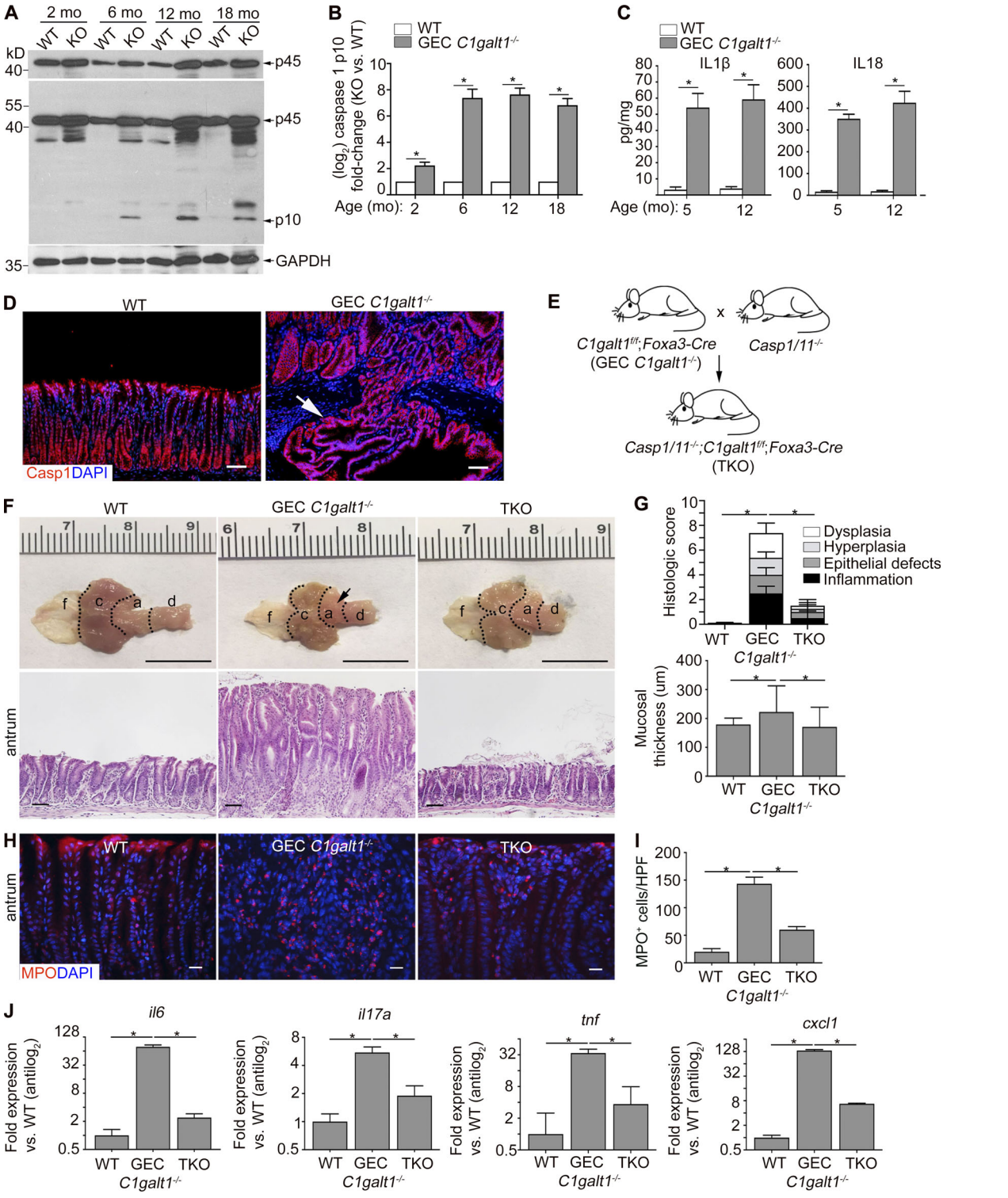

Figure 3. **Chronic gastritis in GEC *C1galt1*$^{-/-}$ mice is driven by mucosal inflammasomes. (A)** Western blot analysis of stomach lysates. p10 is the activated form of Casp1. **(B)** Densitometry of the Casp1 p10 subunit visualized via Western blot of stomach lysates over time. **(C)** Enzyme-linked immunosorbent assay of gastric organ culture supernatants (mean ± SD, *n* = 5 mice/group). **(D)** IF staining for Casp1 in gastric antrum sections. Arrow indicates carcinoma. Scale bars, 50 µm. **(E)** Generation of inflammasome-deficient GEC *C1galt1*$^{-/-}$ mice. **(F)** Representative macroscopic and histological images of murine stomach. Arrow, inflamed region. Scale bars, gross morphology, 1 cm; others, 50 µm. a, antrum; c, corpus; d, duodenum; f, forestomach. **(G)** Histological gastritis score among WT, KO, and TKO mice (means ± SD, *n* = 4–5 mice/group). **(H)** IF for myeloperoxidase (MPO) in gastric antrum sections of 6-mo-old mice. Scale bars, 20 µm. **(I)** Enumeration of MPO$^+$ cells in mucosa (*n* = 4 mice/group). HPF, high-power field. **(J)** qPCR analysis of stomach lysates derived from 6-mo-old mice (means ± SD, *n* = 4–5 mice/group). Data are representative of two independent experiments. *, P < 0.05.

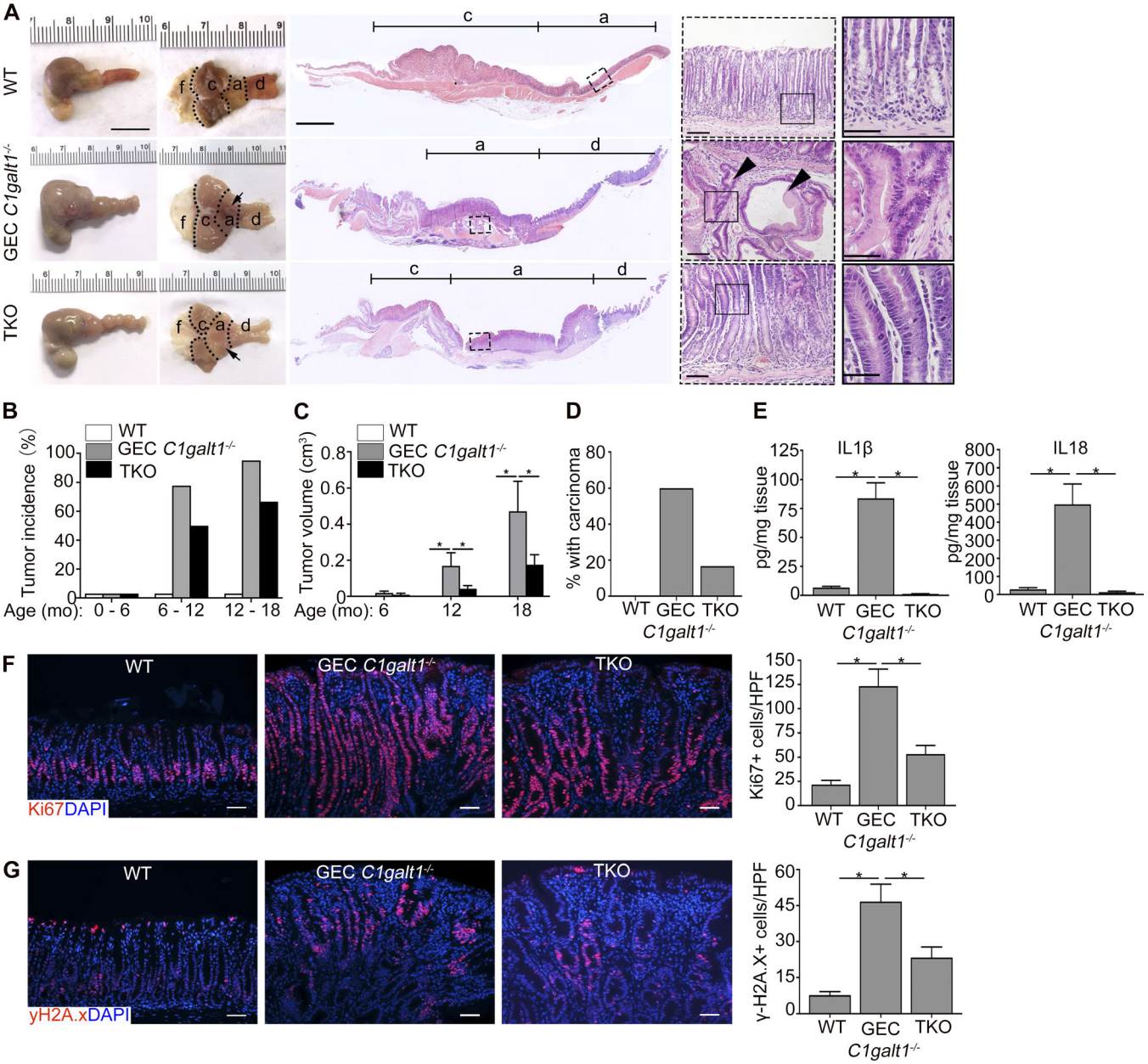

Figure 4. **Mucosal inflammasomes promote gastritis-associated tumorigenesis in GEC *C1galt1*$^{-/-}$ mice. (A)** Representative gross morphology and H&E staining of murine stomach of 12-mo-old mice. Dashed squares mark gastric antrum/tumors. Inset: Magnified images of boxed regions on left. Arrows indicate tumors and arrowheads invasive glands. Scale bars, 1 cm (gross morphology); 200 µm (tiling images); 50 µm (left insets); 25 µm (right inset). a, antrum; c, corpus; d, duodenum; f, forestomach. **(B)** Tumor incidence between littermates or age-matched mice (mean ± SEM). **(C)** Mean tumor volume (mean ± SEM). **(D)** Enumeration of mice with carcinoma of 12–18-mo-old mice (mean ± SEM; *n* = 8–10 mice/group). **(E)** ELISA of organ culture supernatants from 18-mo-old mice (mean ± SEM). **(F and G)** Representative IF staining for Ki-67 (F) and γ-H2A.X (G) in gastric antrum sections of 12-mo-old mice (*n* = 4–5 mice/group). Graphs show quantitation of Ki67^{+} or γ-H2A.X^{+} nuclei. Scale bars, 50 µm. Data are representative of at least two independent cohorts (mean ± SEM). *, P < 0.05. HPF, high-power field.

glands of TKO mice by immunostaining (Fig. S2 A). These results suggest inflammasome-induced gastritis promotes the initiation and progression of gastric tumors in *GEC C1galt1*$^{-/-}$ mice. Inflammasome deficiency did not alter Tn expression in the TKO stomach tissues (Fig. S2 B).

To confirm the association of tumorigenesis with gastritis, we analyzed the gastric antrum epithelial cells among 6-mo-old WT, GEC *C1galt1*$^{-/-}$, and TKO mice, when tumor initiation begins in GEC *C1galt1*$^{-/-}$ mice (Fig. 2), for proliferation and DNA damage responses. As shown in Fig. 4 F, immunostaining for the proliferation marker Ki67 showed significantly reduced epithelial proliferation in TKO versus GEC *C1galt1*$^{-/-}$ mice, but the proliferation level was still elevated versus WT mice. Moreover, we observed reduced staining for phospho-histone 2A.X (γH2A.X), a marker of damaged DNA (Arthur et al., 2012), in TKO mice relative to GEC *C1galt1*$^{-/-}$ mice (Fig. 4 G). These trends were the

same in 12-mo-old mice (Fig. S2, C and D) and were associated with reduced iNOS expression in antrum tissue lysates of TKO versus GEC *C1galt1*$^{-/-}$ mice, a known inducer of DNA damage marked by γH2A.X (Shaked et al., 2012; Fig. S2 E). Notably, Casp1 expression and activation mainly occurred in the antrum, but not in the corpus, of GEC *C1galt1*$^{-/-}$ mice (Fig. S2 F), providing potential insight into why the corpus is unaffected in the absence of O-glycans. These studies indicate that inflammasomes likely accelerate neoplasia in GEC *C1galt1*$^{-/-}$ mice by promoting an inflammatory environment that damages gastric gland cell DNA.

The gastric microbiota is not a significant factor in inflammasome-dependent chronic gastritis and dysplasia in GEC *C1galt1*$^{-/-}$ mice

Our previous work identified the colonic microbiota was essential for Casp1 activation and inflammasome-dependent disease in the colon (Bergstrom et al., 2016). It was unclear if this was the case also in the stomach, since bacterial burdens are expected to be lower due to strongly acidic conditions, yet pathobionts such as *Helicobacter* species may still be present to promote gastric disease (Hitzler et al., 2012). Indeed, we detected several *Helicobacter* species (*H. bilis*, *H. typhlonius*, and *H. hepaticus*) by quantitative RT-PCR (qPCR) of genomic DNA (gDNA) extracted from antrum content of our mouse colonies (Fig. S3 A). To determine whether gastric microbiota contributed to gastritis in our models, we treated 4-wk-old GEC *C1galt1*$^{-/-}$ and WT littermates with broad-spectrum antibiotics (Abxs) for 4 or 16 wk to deplete the gastric microbiota and subsequently assessed gastritis over time (Fig. 5 A). Abx treatment reduced the *H. pylori* populations as detected by qPCR of stomach gDNA, as well as the total bacterial population based on qPCR for universal 16S rRNA gene presence and fluorescence in situ hybridization (FISH) analysis of whole tissue sections with the universal EUB338 probe (Fig. 5, B and C; and Fig. S3 A). Analysis of short-term and prolonged Abx treatment revealed a minimal effect of microbial depletion on the severity or progression of chronic gastritis in GEC *C1galt1*$^{-/-}$ mice, as severe inflammation was seen within the antrum mucosa of short-term Abx-treated versus nontreated mice, and dysplasia was evident even after long-term treatment (Fig. 5 D). We further observed Abx treatment slightly reduced the expression of Casp1 p10 band (Fig. 5, E and F); however, IL1β and IL18 levels in the serum of Abx–treated versus nontreated GEC *C1galt1*$^{-/-}$ mice were similar, both being significantly elevated versus WT controls after short- and long-term Abx treatment (Fig. 5 G). These results suggest a modest role for the gastric microbiota in inflammasome-dependent gastritis and neoplasia in GEC *C1galt1*$^{-/-}$ mice.

Gastric disease in GEC *C1galt1*$^{-/-}$ mice is concurrent with aberrant Muc5AC and Muc1 expression and loss of the gastric mucus layer

O-glycans are major components of gastric mucins, including the membrane-bound Muc1, and the major gastric gel forming mucin Muc5AC (Johansson et al., 2013). We therefore characterized the effect of O-glycan loss on Muc1 and Muc5AC. Staining with periodic acid–Schiff (PAS), which recognizes glycans, revealed that GEC *C1galt1*$^{-/-}$ mice had a loss of the mucus gel layer in corpus and antrum versus age-matched and littermate WT mice at 8 wk of age (Fig. 6 A). Consistent with this, staining with *Ulex europaeus* agglutinin-1 (UEA-1), which detects the neutral glycan fucose, showed reduced levels in GEC *C1galt1*$^{-/-}$ versus WT, more so in the antrum than the corpus (Fig. 6 A). Immunostaining revealed increased overall expression of Muc1 in GEC *C1galt1*$^{-/-}$ mice, mainly in the antrum (Fig. 6 A). In contrast, dual immunostaining for Muc5AC and Tn antigen revealed a dramatic decrease in Muc5AC staining in the gastric antrum in GEC *C1galt1*$^{-/-}$ versus WT mice, concomitant with increased Tn (Fig. 6 A). As expected, Tn antigen was barely detectable in WT tissues (Fig. 6 A). A longitudinal study showed Muc1 expression increased while Muc5AC expression decreased in GEC *C1galt1*$^{-/-}$ versus WT mice over time (Fig. 6 A). qPCR analysis of the *Muc5ac* gene expression in the antrum showed an increase in GEC *C1galt1*$^{-/-}$ versus WT tissues over time, with expression levels discordant with Muc5AC protein in GEC *C1galt1*$^{-/-}$ mice at 8 wk of age (Fig. S3 B). This suggested that a loss of core 1–derived O-glycans impairs gastric mucin synthesis at a posttranslational level, likely due to impaired intracellular trafficking and/or defective stability. We also examined expression of two members of the Trefoil-factor family, Tff1 and Tff2, which interact with human gastric mucins MUC5AC and MUC6, respectively (Hoffmann, 2015; Ruchaud-Sparagano et al., 2004) and play important roles in protection against gastritis and gastric cancer in mice and humans (Fox et al., 2007; Lefebvre et al., 1996; Peterson et al., 2010; Soutto et al., 2011); Tff1, a negative regulator of NF-κB signaling, but not Tff2, was reduced in GEC *C1galt1*$^{-/-}$ mice at 8 wk of age (Fig. S3 C). These results confirm that spontaneous gastritis was closely associated with aberrant presentation of the mucosal barrier in GEC *C1galt1*$^{-/-}$ mice.

Antrum-specific disease in *GEC C1galt1*$^{-/-}$ mice is associated with altered gastric acid homeostasis

Gastric mucins protect mucosa from gastric acids (Holmén Larsson et al., 2013). Previous studies have shown acidic environments can activate Casp1 (Rajamäki et al., 2013). We tested whether blocking acid production ameliorates Casp1 activation and disease development, starting in mice 4 mo of age (established gastritis; Fig. 7 A). We found both long-term and short-term treatments of omeprazole (OME), an established proton pump inhibitor, had a considerable ameliorative effect on disease severity (Fig. 7 B and data not shown). The short-term treatment also reduced the Casp1 activation in the antrum of GEC *C1galt1*$^{-/-}$ mice despite some variations (Fig. 7 C). These results suggest that the acidic microenvironment contributes to Casp1-mediated gastric disease in our mouse model. Unexpectedly, we discovered that GEC *C1galt1*$^{-/-}$ mice had a higher gastric pH (pH ∼4) at baseline, and OME treatment did not significantly increase GEC *C1galt1*$^{-/-}$ gastric pH compared with WT littermates (Fig. 7 D). Although these results indicate that core 1 O-glycosylation is essential for gastric acid homeostasis in the stomach, they suggest a mechanism other than, or in addition to, inhibiting gastric acid contributes to the OME-mediated decrease of inflammasome-dependent GEC *C1galt1*$^{-/-}$ gastritis. The precise mechanism of Casp1 activation in GEC *C1galt1*$^{-/-}$ mice remains to be studied in the future.

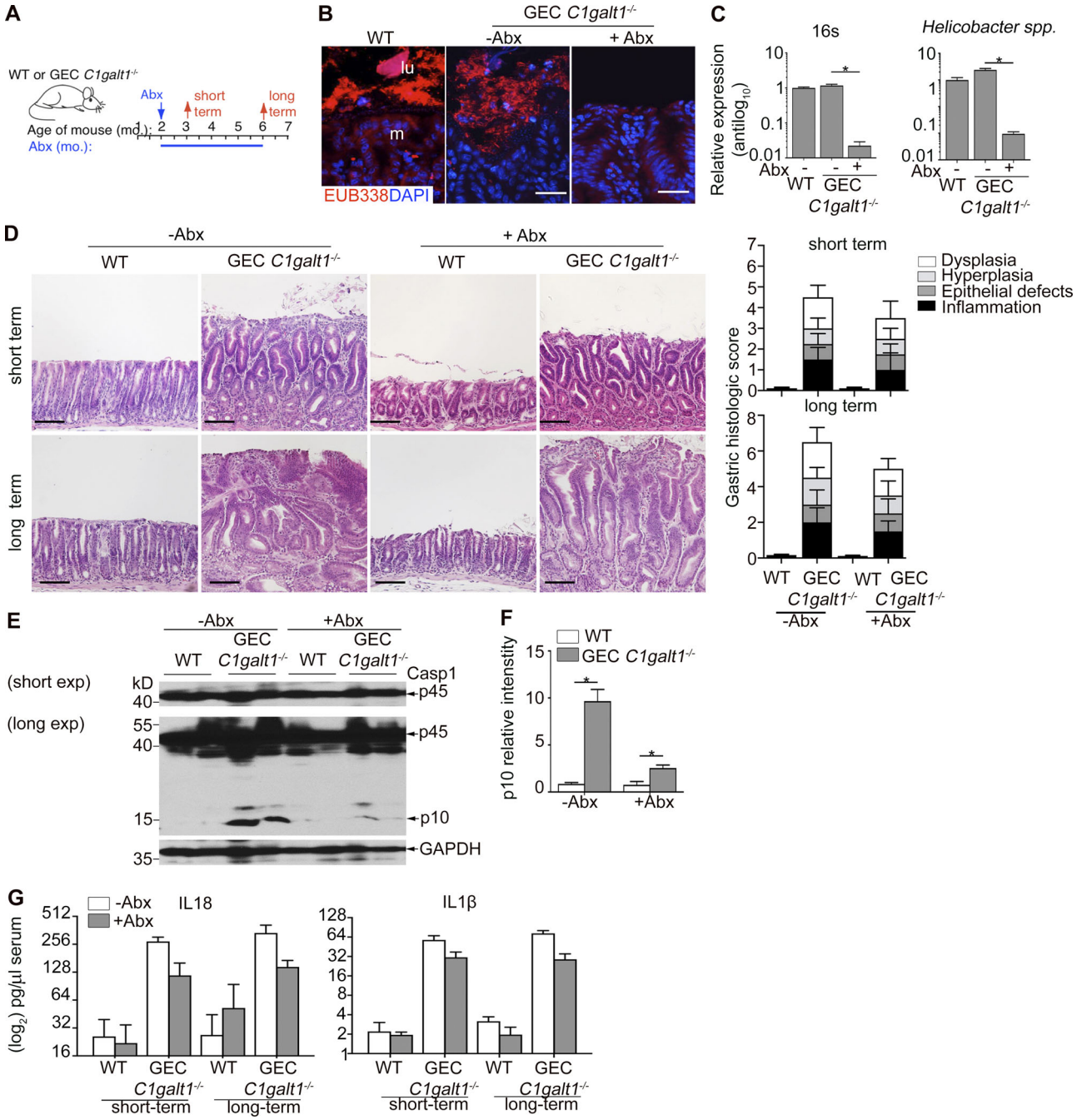

Figure 5. **The gastric microbiota is dispensable for disease development in GEC *C1galt1*$^{-/-}$ mice. (A)** Abx treatment regimen. **(B)** FISH using the EUB338 probe on gastric sections of 6-mo-old mice. Dashed line, interface between lumen (lu) and mucosa (m). Scale bars, 20 µm. **(C)** Representative qPCR for the 16S ribosomal RNA gene from genomic DNA extracted from stomach contents (mean ± SEM; *n* = 5 mice/group). **(D)** H&E of antrum sections. Graphs on right; gastritis activity index. Scale bars, 50 µm. **(E)** Western blot analysis of stomach lysates. **(F)** Densitometry of Casp1 p10 subunit in Western blot (mean ± SEM). **(G)** ELISA for IL1β and IL18 in serum. Results are representative of three or four mice per group (mean ± SEM). *, P < 0.05.

Tn antigen is not sufficient to promote gastric epithelial hyperplasia

Exposure of abnormal glycans, such as truncated O-glycans Tn antigen, is associated with cancer cell development in vitro (Freitas et al., 2019; Radhakrishnan et al., 2014). We asked whether antrum epithelial cell–intrinsic defects caused by Tn exposure contributes to disease development. We tested this by culturing organoids from stem cell–containing glands isolated from the antrum of WT versus the inflamed Tn-positive GEC *C1galt1*$^{-/-}$ antrum (Miyoshi and Stappenbeck, 2013). The primary GEC *C1galt1*$^{-/-}$ organoids grew faster than those from the WT littermate controls (Fig. S4 A). However, after passage, the growth rates of WT versus GEC *C1galt1*$^{-/-}$ organoids were equalized (Fig. S4 B). These results suggest that gastric epithelial stem cells derived from inflamed tissue soon lost their increased proliferative advantage outside an overt inflammatory milieu

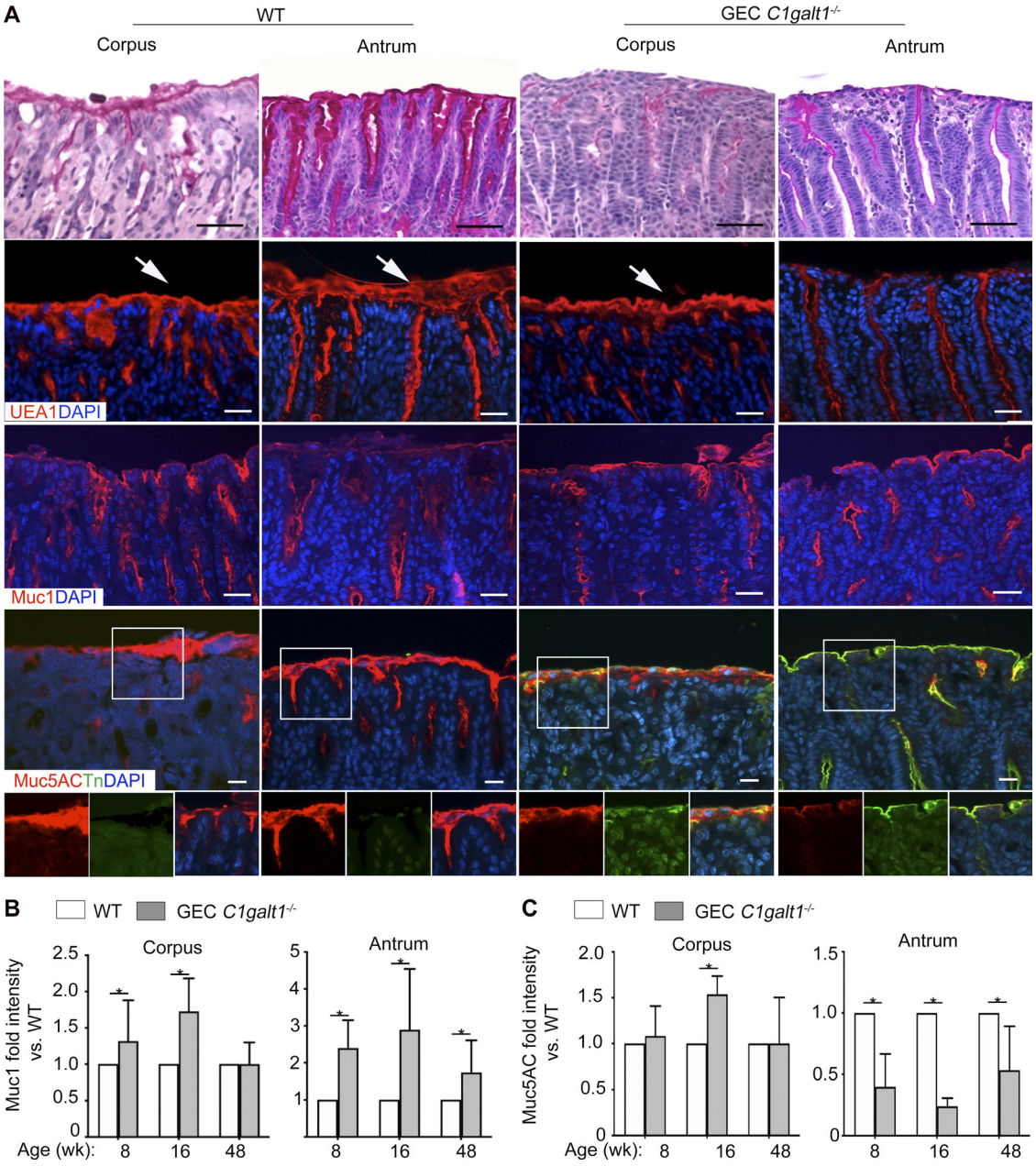

Figure 6. **Spontaneous gastritis in GEC *C1galt1*$^{-/-}$ mice is associated with dysregulated Muc1 and Muc5AC expression. (A)** Representative images of formalin-fixed stomach regions stained with different markers as indicated. Arrows show the surface mucus layer. Data are representative of 10 mice per group pooled from at least two cohorts (n = 8–10 mice/group for PAS staining, UEA1, and Muc5AC; n = 4 mice/group for Muc1 staining). Scale bars, 25 µm. **(B and C)** Quantification of Muc1 and Muc5AC staining (mean ± SD; *, P < 0.05).

despite Tn expression. Thus, Tn exposure does not appear to be sufficient to intrinsically alter gastric stem cell activity. This ex vivo result is supported by in vivo results after OME treatment, which reproducibly reduces inflammation despite persistent expression of Tn antigen in GEC *C1galt1*$^{-/-}$ gastric antrum (Fig. S4 C).

Truncated O-glycans and inflammasome activation are associated with gastritis and gastric cancer in patients

Our results show that O-glycan truncation to Tn antigen due to loss of C1galt1 activity is a cause of gastritis and gastric cancer by promoting inflammasome activation in the gastric antrum in mice. To address the clinical relevance of these findings, we stained tissue arrays containing a panel of gastric tissues from healthy, gastritis, or gastric cancer patients with an antibody to Tn antigen. Our results showed that Tn antigen was exposed in 75% of gastritis tissues (9 of 12), 69.5% of gastric tumor samples (41 of 59) relative to 40.7% of paired adjacent nontumor samples (18 of 59) and 16.7% of healthy tissues (1 of 6; Fig. 8, A and B). Notably, male gastric cancers tended to have a higher frequency of Tn expression (~78%) than female (56.5%); the antrum was the most frequent site of tumors and was associated with the

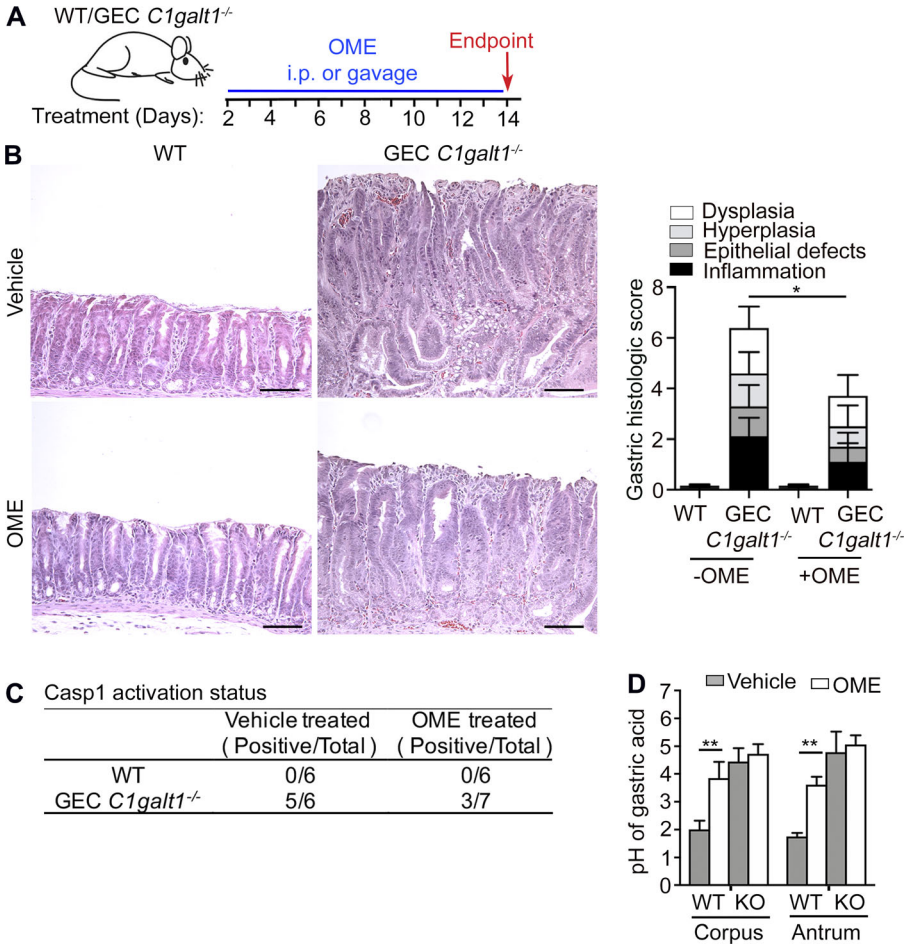

Figure 7. **GEC *C1galt1*$^{-/-}$ exhibit impaired gastric acid homeostasis associated with disease that is partly modulated by proton-pump inhibition. (A)** Experimental design strategy. **(B)** H&E of antrum sections and histological score. Scale bars, 50 µm. **(C)** Western blot analysis of Casp1 activation in antrum in response to OME treatment (number of mice with a p10-positive band/total number of mice). **(D)** pH measurement after 14 d OME treatment. Results are representative of two independent experiments; *n* = 6–7 mice per group. Data are mean ± SD. *, P < 0.05; **, P < 0.01.

highest Tn expression (Table S1). Furthermore, Tn expression was correlated with *H. pylori* infection, inflammation, and progression of the tumors, but not with age (Table S1).

To examine the role of inflammasome activation in gastric diseases, we analyzed tissue sections and fresh gastric samples from gastric cancer patients and healthy controls for CASP1 expression by immunostaining and Western blot analysis. As shown in Fig. 8 C, CASP1 staining was detected in both cytoplasmic and nuclear compartments of gastric epithelial and stromal cells in patients with gastritis and tumors (Fig. 8 C, arrow and arrowheads). The nuclear staining is consistent with a reported finding in other cells (Wang et al., 2016). The expression level of CASP1 was associated with the degree of inflammation, tumor differentiation, progression, and to a lesser extent with *H. pylori* infection, but not with gender, age, or tumor location in the stomach (Table S2). Tn and CASP1 expression levels were correlated (Table S3). With respect to CASP1 activation status in gastric cancer patients, the activated form of CASP1 p10 was observed in 63.33% of gastric cancer tissue samples (19 of 30), but not in healthy controls (0 of 6; Fig. 8 D). Like CASP1 expression, p10 was positively correlated with degree of inflammation, *H. pylori* infection status, tumor differentiation, and progression (the tumor node metastasis classification system, TNM) of gastric cancer patients, but not gender, age, or tumor location (Table S4; P < 0.05). These studies indicate that O-glycan truncation and activation of the inflammasome is closely associated with the pathogenesis of human gastritis and gastric cancer.

Discussion

Aberrant expression of mucin-type O-glycosylation has been observed in gastric cancer progression (Barresi et al., 2001; Duarte et al., 2016; Heneghan et al., 1998; Lindén et al., 2008; Persson et al., 2017), but whether and how truncation of O-glycosylation contributes to the pathogenesis of this disease is unclear. In this study, we show that deletion of core 1–derived O-glycans leads to impaired gastric mucin function and results in spontaneous inflammation-associated gastritis and gastric cancer. The disease was largely dependent upon gastric mucosal inflammasomes, which are activated in a microbiota/*Helicobacter*–independent manner likely due to a defective O-glycan–dependent gastric mucus barrier and altered gastric acid homeostasis. O-glycan truncation and activation of inflammasomes were also observed in gastritis and gastric cancer patients. Collectively, these results support an important primary role of defective O-glycosylation in the pathogenesis of gastritis and gastritis-associated cancer.

In our model, the gene *C1GalT1* required for the biosynthesis of core 1 O-glycans, on which major complex O-glycans are built (Ju and Cummings, 2002), is deleted, leading to the exposure of the Tn structure. Based on Tn expression, no other complex

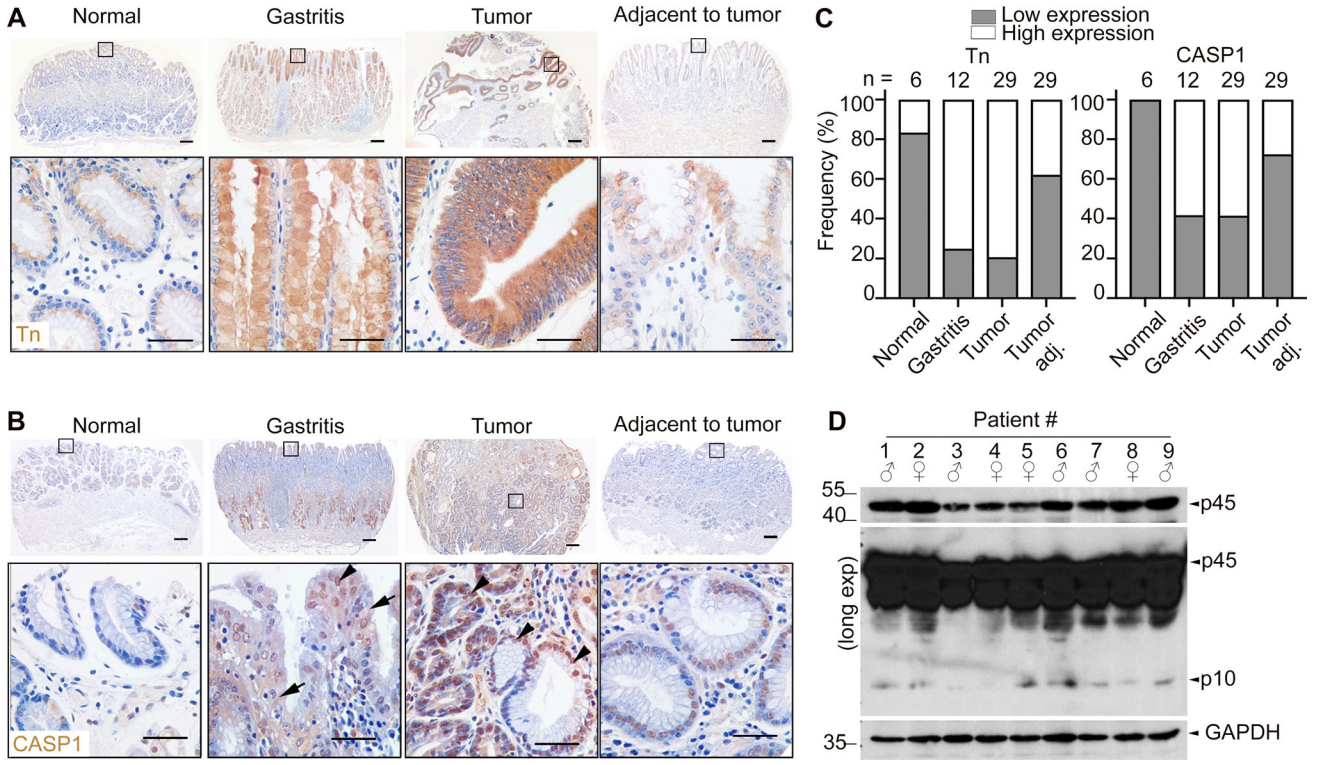

Figure 8. **Truncated O-glycans and inflammasome activation are associated with gastritis and gastric cancer in human patients. (A)** IHC for Tn-antigen in human gastric tissue sections. Scale bars, 50 µm (upper panel) and 20 µm (inset). **(B)** IHC for Casp1 in human gastric tissue sections. Arrows indicate cytoplasmic staining, and arrowheads indicate nuclear staining. **(C)** Frequency of low versus high Tn expression status (defined in Materials and methods) in tissue in relation to disease status. **(D)** Western blot analysis of CASP1 expression in human gastric cancer tissue samples. Each lane represents one gastric cancer tissue sample. Exp., exposure.

O-glycan structures appear to have been synthesized to compensate for the loss of core 1. A previous study shows that α1,4 linked GlcNAc structure (α-GlcNAc) plays a role in glycan-dependent gastric homeostasis (Karasawa et al., 2012). Functionally, α-GlcNAc can have a direct antimicrobial activity against the causative agent of gastritis-associated cancer, *H. pylori*, by inhibiting synthesis of its cell wall (Kawakubo et al., 2004). Interestingly, similar to gastric epithelial *C1GalT1* deficiency, loss of *a4GnT*, the glycosyltransferase responsible for synthesis of α-GlcNAc, also leads to spontaneous gastritis-associated cancer in mice localized to the pyloric epithelial cells of the antrum, although this is independent of its effects on *H. pylori* (Karasawa et al., 2012). Since loss of *C1GalT1* will likely cause deficiency of α-GlcNAc, it is possible that our phenotype is linked to deficiency of this glycan. However, important differences in the pathologies of GEC *C1galt1*$^{-/-}$ and *a4GnT* $^{-/-}$ mice argue for a different mechanism underlying the gastric pathogenesis in these lines. For example, the disease in *a4GnT*$^{-/-}$ mice progresses much more rapidly, with tumors evident by 5 wk of age (Karasawa et al., 2012), whereas in GEC *C1galt1*$^{-/-}$ mice, tumors do not develop until after 60 wk (present study). The basis for these differences is unclear; however, it is notable that there is a remodeling of the overall O-glycan structures in the absence of α4GnT (Karasawa et al., 2012), whereas the simple glycan structure Tn antigen dominates in the absence of *C1GalT1*. These differences in O-glycosylation profiles may fundamentally alter cell-intrinsic functions, for example those of stem cells (Nishihara, 2018). Further, we observed the effect of *C1galt1* loss impacts the entire gland epithelium, whereas α4GnT deficiency impacts the deep gland (where Muc6 is expressed; Karasawa et al., 2012). Therefore, it is likely the lack of complex O-glycosylation due to core 1 O-glycan loss is affecting events at the mucosal surface (where Muc5AC is expressed). Importantly, both glycan truncation and alterations such as αGlcNAc deficiency are reported in gastric cancer (David et al., 1992; Duarte et al., 2016; Li et al., 2018; Mereiter et al., 2018; Springer, 1984; Werther et al., 1994), highlighting the diverse means by which O-glycans and their alterations contribute to gastric homeostasis and disease.

Our results show gastritis and gastric cancer was mediated by mucosal inflammasomes. This is similar to the colon, where Casp1-depedent inflammasomes promote colitis-associated cancer in the absence of core 1– and 3–derived O-glycans (Bergstrom et al., 2016). Inflammasomes, via their substrates like IL1β and IL18, have been implicated in the progression of gastritis and gastritis-associated cancer (Hitzler et al., 2012; Kameoka et al., 2016; Koch and Müller, 2015; Ng et al., 2016; Pachathundikandi et al., 2016). This is usually in the context of chronic infection by the *Helicobacter* species, which are thought to drive gastritis through the NLRP3 inflammasome (Koch and Müller, 2015). Whether *Helicobacter* species are involved in our model is unclear; however, our broad-spectrum Abx treatment

argues against, but does not rule out, this scenario. Interestingly, the *Helicobacter*-independent gastric disease in αGlcNAc-deficient mice is associated with excessive IL1β, implicating inflammasome activity as a potential driving force for pathogenesis in αGlcNAc-deficient mice (Karasawa et al., 2012) and suggesting that O-glycans in general protect against idiopathic gastritis driven by this pathway. In some cases, inflammasome signaling can have a regulatory effect on gastritis and ensuing neoplasia, dependent on its downstream effectors such as IL1β, which drives the disease, or IL18, which is thought to ameliorate it (Hitzler et al., 2012). Both inflammasome substrates are induced in our model, and it is likely IL1β is the driver in our context based on the disease severity.

It is notable that the antrum, the major site of disease in our model, is also a primary region for *H. pylori*–induced gastritis and gastric cancer in humans (Marshall, 1995). Although our model appears to be independent of *Helicobacter* species, the one unifying factor in both settings is the pathological role of hyperactive inflammasome signaling (Hitzler et al., 2012; Kameoka et al., 2016; Koch and Müller, 2015; Ng et al., 2016; Pachathundikandi et al., 2016), along with O-glycan truncation, as described in the present study. One insight into why the antrum is susceptible to gastritis may be linked to our finding that the relative expression of Casp1 and its overall activation was markedly less in the corpus than the antrum of mice (regardless of core 1 O-glycosylation status). Whether this is true in humans has yet to be determined.

The primary defect of the antrum of GEC *C1galt1*$^{-/-}$ mice is dysregulated expression of Muc5AC and Muc1. At baseline, the gastric mucosa contains mostly neutral glycans (Duarte et al., 2016). Unexpectedly, Muc5AC protein expression is nearly abolished in the gastric tissues of GEC *C1galt1*$^{-/-}$ mice, which may be due to abnormal intracellular trafficking and/or degradation in the absence of normal O-glycosylation. This is different from that in the colon, where Muc2, the principal gel-forming mucin of the colon, is still abundant in goblet cells but is lost in the lumen due to rapid degradation of O-glycan–deficient Muc2 by the microbiota (Bergstrom et al., 2017). The membrane-bound Muc1 expression seemed to increase on the antrum surface of GEC *C1galt1*$^{-/-}$ mice relative to controls. Muc1 plays many protective roles during gastritis and *Helicobacter* infection (Balmaña et al., 2018; Lindén et al., 2009; McGuckin et al., 2007; Ng et al., 2016), but these functions are likely impaired by O-glycan defects. Taken together, defective expression and/or function of key mucins Muc5AC and Muc1 contribute to the impaired barrier of the gastric mucosa, likely positively influencing gastric inflammation and tumor development.

Gastric acid has a potent ability to damage host and microbial cells. The mucus layer covering gastric mucosa is important in the preservation of gastric homeostasis in the presence of acids. There is a pH gradient in the mucus; a low pH (pH 1–2) exists at the luminal side of the mucus, while a neutral pH (pH 6–7) exists at the basal side toward the epithelial surface due to bicarbonate production by gastric epithelia (Schade et al., 1994). Secreted acid from parietal cells is transported through channel-like structures within the mucus. These channels are likely generated by high intraglandular pressures forcing acid through the mucus gel toward the lumen of the stomach (Johansson et al., 2000). Acid does not move back through the channels, likely due to factors such as differences in luminal versus glandular pressures (Bhaskar et al., 1991, 1992; Johansson et al., 2000). Ultimately, a steep pH gradient through the mucus is maintained (Phillipson et al., 2002; Schade et al., 1994). Interestingly, the basal gastric pH of GEC *C1galt1*$^{-/-}$ mice was pH ∼4–5, which is higher than that of WT mice. This unexpected result supports that the diffusion barrier capacity of the O-glycan–rich mucus was disrupted, either directly, through loss of the mucus-gel–forming mucin Muc5AC on the antrum surface, or indirectly, by affecting corpus parietal cell functions. This result highlights the importance of O-glycosylation in preservation of gastric homeostasis.

One caveat of our study is that our TKO lines are lacking both Casp1 and Casp11 due to a loss-of-function passenger mutation in the Casp11-encoding *Casp4* gene on the *Casp1*$^{-/-}$ knockout background (Kayagaki et al., 2011); therefore, it is unclear which of these inflammatory caspases are contributing to the disease. The strong Casp1 expression in epithelium in the present study, even in carcinoma, suggests at least Casp1 is an important driver. Crossing *Foxa3-Cre* with mice harboring both floxed *C1galt1* and *Casp1* alleles will determine this more conclusively in the future. Regardless, our data suggest that gastric inflammasomes are a therapeutic target for the treatment of gastritis.

Although aberrant glycosylation, including loss of complex O-glycans, occurs in patients with gastric cancer (Fu et al., 2016; Mereiter et al., 2018), its exposure level in human gastritis remains unclear. It was shown that Tn-antigen exposure did not change relative to disease status in a patient cohort, being limited to the supranuclear (Golgi-localized region; Barresi et al., 2001). Our results show that Tn is expressed in stomach tissues of patients with gastric cancer based on a reliable anti-Tn monoclonal antibody BaGs6 (Sun et al., 2018). Although our results do not support that the Tn exposure itself is sufficient to cause tumor development, our findings in various mouse models do demonstrate that O-glycan defects cause gastritis and gastritis-associated cancer and link it directly to inflammasome activation in mice and people. Interestingly, although our population size was relatively small and limited to a single ethnic population (Chinese), we found higher incidence of gastric cancer in male versus female cohorts. This interesting observation is of relevance, since COSMC, a molecule chaperone essential for C1GalT1 activity (Wang et al., 2010), is X linked. *Cosmc* mutations have been found in many types of human adenocarcinomas. Future studies to detect *Cosmc* mutation status in gastric cancer patient samples would be important to determine the mechanistic relationship between X-linked glycosylation pathways such as core 1 O-glycosylation and susceptibility of gastric diseases.

In conclusion, our results emphasize the essential role of gastric mucin-type O-glycosylation in gastric homeostasis and protection from chronic gastritis-associated cancer. Our results also suggest that inhibition of key inflammatory pathways mediated by inflammasome activation (Casp1 dependent) may reduce the incidence of carcinogenesis in patients with gastritis. Targeting either aberrant gastric mucin-type O-glycosylation or

mucosal inflammasomes may serve as potential therapeutics in human gastric cancer in the future.

Materials and methods

Generation of mice

Mice lacking gastric core 1–derived O-glycans (*C1galt1*$^{f/f}$;*Foxa3*Cre or GEC *C1galt1*$^{-/-}$) were generated by breeding *C1galt1*$^{f/f}$ mice with Foxa3Cre transgenic mice. GEC *C1galt1*$^{-/-}$ mice were crossed with mice lacking both Casp1 and Casp11 (*Casp1*/Casp4^{del}) to generate mice lacking canonical and noncanonical inflammasomes (TKO). All mice were from a mixed B6/129 or B6/129/NOD background. WT littermates were used as controls. Male and female mice were used throughout the study. Mice were housed in a specific pathogen–free barrier facility and fed standard chow (PicoLab Rodent Diet 20; LabDiet). All animal studies were approved by the Institutional Animal Care and Use Committee of the Oklahoma Medical Research Foundation.

Histology

For histology, stomach tissues were harvested from mice and fixed with 10% neutral-buffered formalin or in Carnoy's fixative (60% methanol, 30% chloroform, and 10% acetic acid) before paraffin embedding. Paraffin-embedded sections (5 µm) were stained with H&E or PAS. Images were taken with a Nikon Eclipse E600 microscope equipped with a Nikon DS-2Mv camera with 20× (NA 0.75) and 40× (NA 0.75) objectives using the software NIS Freeware 2.10 (all from Nikon Instruments). Histological scoring at each stage of disease (gastritis, dysplasia, and carcinoma) was performed according to a previously established system (Rodgers, 2012). A summary of the parameters is provided in Table S5.

Immunostaining

Immunofluorescence (IF) staining was performed as described previously (Bergstrom et al., 2016). Briefly, 5-µm-thick formalin or Carnoy's-fixed paraffin-embedded sections were deparaffinized and rehydrated. Where required, antigen retrieval was performed by heating sections between 95°C and 100°C for 23 min in Antigen Unmasking Solution (H-3300; Vector Laboratories). Blocking of nonspecific antibody binding was performed using serum-free protein block (008120, 10 min, room temperature; Life Technologies). For biotinylated primary antibodies, streptavidin/biotin blocking (SP-2002; Vector Laboratories) was performed before nonspecific antibody block. Following blocking, sections were incubated with primary antibody in a humidified chamber overnight at 4°C or 2 h at ambient temperature. After washing, the sections were incubated with a fluorochrome-conjugated secondary antibody (8 µg/ml) or streptavidin (5 µg/ml) for 1 h in the dark at room temperature. The primary antibodies used were biotin-conjugated mouse anti-Muc5AC (1:100, MA5-12175; Thermo Fisher Scientific), rabbit anti-myeloperoxidase (5 mg/ml, PA5-16672; Thermo Fisher Scientific), rat anti-F4/80 (5 mg/ml, clone C1:A3-1; Bio-Rad), rabbit anti-Ki67 (1:100, RM-9106-S0; Thermo Fisher Scientific), rabbit anti-γH2A.X (1:100, #9718; Cell Signaling Technologies), and rabbit anti-Casp1 (1:200, ab108362; Abcam) in a humidified chamber overnight at 4°C or 2 h at ambient temperature. Detection reagents were DyLight 488–labeled streptavidin (5 µg/ml, #21832; Thermo Fisher Scientific), Alexa Fluor 488–labeled goat anti-rat IgG (1:50, #111-545-003; Jackson ImmunoResearch Laboratories), and Alexa Fluor 594–labeled goat anti-rabbit IgG (5 µg/ml, #111-585-003; Jackson ImmunoResearch Laboratories). Sections were counterstained with 25 ng/ml 4,6-diamidino-2-phenylindole and mounted using PermaFluor antifade (Thermo Fisher Scientific). For epifluorescence imaging, specimens were analyzed by a Nikon Eclipse 80*i* microscope equipped with a Nikon DS-Qi1MC camera with 20× (NA 0.5) and 40× (NA 0.75) objectives operating through NIS Elements AR software (version 3.0). Tn-antigen staining was performed by IHC staining using the BaGs6 monoclonal antibody (1:125, clone Ca3638; Wang et al., 2010). Species-specific, isotype control IgG or nonprimary antibody–treated sections were used for negative controls.

Enumeration of immunostaining

For each section, three to five different high-powered microscopic fields (×40) were chosen randomly to count MPO$^+$ cells in gastric mucosa. For proliferation analysis, immunostaining for Ki-67 was performed, and the average number of Ki-67$^+$ cells per high-power field was determined for each mouse, followed by calculation of the mean of these averages among all mice in each respective experimental group. An identical approach with γH2A.X staining was used to assess DNA damage. All the enumeration was performed under blinded conditions using ImageJ software (version 1.51).

Protein extraction and Western blot

Protein extraction from gastric tissues was performed as described for intestinal tissues (Bergstrom et al., 2016). Briefly, ∼0.5 cm^2 mouse antrum or human gastric tissue was placed in radioimmunoprecipitation assay buffer with protease inhibitors, lysed by bead milling, cleared by centrifugation, and quantified by the Bio-Rad Dc Protein Assay. 20–50 µg protein was used for 15% SDS-PAGE under denaturing conditions and transferred to a polyvinylidene difluoride membrane (20 V, 45 min; Thermo Fisher Scientific) using a Transblot SD Semidry Transfer Cell (Bio-Rad). Membranes were blocked with 5% skim milk in TBST (Tris-buffered saline with 0.05% Tween 20) and incubated with primary antibody overnight at 4°C or 2 h at ambient temp in TBST with 5% skim milk. Detection was performed with HRP-conjugated goat anti-rabbit IgG (0.2 µg/ml) or anti-mouse IgG (0.2 µg/ml), followed by chemiluminescence (SuperSignal West Pico Chemiluminescent Substrate kit; Thermo Fisher Scientific), and imaged using the SynGene G:Box gel doc system (Syngene) or via film. Primary antibodies were rabbit anti-Casp1 p10 (1:1,000; ab108362; Abcam), mouse anti-NOS2 (C-11; 1:1,000; sc-7271; Santa Cruz), and rabbit anti-ASC (1:2,000; sc-22514R; Santa Cruz). Rabbit anti-GAPDH (1:5,000; sc-25778; Santa Cruz) was used as a loading control on blots stripped with ReBlot (G-Biosciences). Densitometry of the Casp1 p10 was performed as previously described (Bergstrom et al., 2016).

Nucleic acid extraction and qPCR

Total RNA was extracted from mouse tissue as previously described for intestinal tissues (Bergstrom et al., 2016). Briefly, total RNA was extracted from antrum tissues using the RNeasy kit (Qiagen) and reverse transcribed using the Omniscript Reverse-Transcription kit (Qiagen) according to the manufacturer's protocols. Stomach gDNA was isolated using the Qiagen Stool Mini Kit. qPCR was performed using 2× iQ MasterMix and a CFX-96 system (Bio-Rad). Primer sequences are previously published (Bergstrom et al., 2016). *Helicobacter*-specific primer sequences were obtained from (Feng et al., 2005). Expression analysis was performed using the Bio-Rad CFX manager 3.0 (using the $^{\Delta}$Ct method for normalized expression, and $^{\Delta\Delta}$Ct for relative normalized expression). All relative normalized expression data used 18S ribosomal RNA messenger RNA or (*Hprt*) hypoxanthine guanine phosphoribosyltransferase messenger RNA as internal controls, each providing similar results. Primer sequences are listed in Table S6.

Abx treatment and bacterial analysis

Abx treatment was performed as previously described (Gao et al., 2016) for indicated times (see Results). Briefly, 4-wk-old mice were given filter-sterilized (0.22 µm) tap water supplemented with ampicillin (1 g/liter), vancomycin (500 mg/liter), neomycin sulfate (1 g/liter), metronidazole (1 g/liter), and sucrose (1 g/liter). Control mice were given drinking water supplemented with 1 g/liter sucrose. All Abxs were purchased from MP Biochemicals except metronidazole (Sigma-Aldrich). Abx effectiveness was determined through qPCR for the universal region of the gene encoding 16S rRNA on gDNA extracted from stomach contents and feces. Primer sequences are listed in Table S7.

FISH

For FISH, food-containing stomach sections fixed with Carnoy's fixative were incubated with Texas red–conjugated universal bacterial probe EUB338 (5′-GCTGCCTCCCGTAGGAGT-3′; bp 337–354 in bacterial EU622773) or with a nonspecific probe (NON338; 5′-ACTCCTACGGGAGGCAGC-3′) as a negative control (both from Eurofins MWG Operon) in hybridization buffer (20 mmol/liter Tris-HCl, pH 7.4, 0.9 mol/liter NaCl, and 0.1% sodium dodecyl sulfate) at 37°C overnight. The sections were rinsed in wash buffer (20 mmol/liter Tris-HCl, pH 7.4, and 0.9 mol/liter NaCl) at 37°C for 15 min. Sections were counterstained and imaged as described above.

Organ culture and ELISA

Longitudinally open stomachs were washed in sterile PBS, and 0.5 × 0.5-cm gastric antrum tissues (same region in all mice) were cut into three or four pieces and placed in 1 ml RPMI containing 1% penicillin/streptomycin/glutamate and placed in a humidified incubator (37°C, 5% CO_2) for 24 h. Supernatants were collected, spun at 10,000 rpm for 2 min to remove debris, and supernatant was collected and supplemented with Halt protease inhibitors (1×) and then stored at −80°C until further use. Remaining tissues were taken, blotted dry, and weighed. A total of 100 µl supernatant was analyzed by ELISA using the IL18 ELISA (MBL) and IL1β ELISA (#88-7013; Invitrogen) kits, each according to the manufacturer's instructions. Absolute values were determined from standards, and final values were obtained after normalizing to tissue weight.

Patient sample analysis

Informed consent was obtained according to a patient study approved by the Institutional Review Board and Ethics Committee of the First Affiliated Hospital of Soochow University (Suzhou, China). De-identified postoperation fresh tissue samples of human gastric cancer patients and healthy stomach tissue samples were obtained from the Department of General Surgery of the First Affiliated Hospital of Soochow University. All patients had accurate pathology diagnosis and underwent surgery without chemotherapy or radiotherapy before operation. Information regarding the 30 human gastric cancer patients is described in Table S1. Tissues lysates were prepared as described above.

Tissue microarray chips containing 6 normal gastric tissue samples, 12 gastritis tissue samples, 29 pairs of gastric cancer tissue samples matched to their adjacent nontumor stomach tissue samples, 14 metastatic lymph nodes, 11 distant metastatic organs, and the associated clinicopathological information were purchased from Shanghai OUTDO Biotech. IHC of Tn and Casp1 were performed using biotinylated anti-Tn and anti-Casp1 (HPA003056; Sigma-Aldrich) antibody, respectively, as described above. The total score (values 0–12) of protein expression was calculated by multiplying the percentage of immunopositive areas (0–25% = 1, 26–50% = 2, 51–75% = 3, >75% = 4) and immunostaining intensity (negative = 0, weak = 1, moderate = 2, or strong = 3). A score ≥6 defined high expression, while a score <6 defined low expression.

OME treatment

For long-term studies, WT and GEC *C1galt1*$^{-/-}$ mice (~2 mo, littermate pairs) mice were given 0.02% wt/wt OME in a base diet identical to control mice (TestDiet 5WRM, #1818774–203; Saqui-Salces et al., 2017) and i.p. injection of OME (#73590-58-6; Cayman Chemical) in dimethylformamide at a concentration of 20 mg/ml diluted 1:9 with sterile PBS (final concentration, 2 mg/ml, 20 mg/kg for injection). For short-term studies, WT and GEC *C1galt1*$^{-/-}$ mice (4 mo old; littermate pairs were analyzed) were administrated with OME or vehicle by i.p. and gavage. For gavage, OME was suspended directly into sunflower oil (20 mg/kg).

Measurement of murine gastric acid pH

WT and GEC *C1galt1*$^{-/-}$ mice treated by OME or vehicle were i.p. injected with OME (20 mg/kg) before the start of the experiment. At predetermined times, mice were euthanized, and stomachs were excised and cut open longitudinally. Luminal contents were collected carefully into 1.5-ml tubes from the corpus and antrum and centrifuged at 15,000 rpm for 5 min. After centrifugation, the pH of the supernatant (10–20 µl) was immediately measured using an Orion 9863BN Micro pH electrode (Thermo Fisher Scientific). Care was taken during pH measurement to fully immerse the pH probe in the liquid contents. pH standards were used for calibration in small volumes (10–20 µl) to confirm accuracy of readings.

Organoid culture

Antral pits were isolated and cultured using an established method (Miyoshi and Stappenbeck, 2013; Yi et al., 2019). Briefly, isolated pits were embedded in Matrigel on ice and seeded in a 24-well plate. 500 µl culture medium was added, and organoids were cultured at 37°C in cell culture incubator. At day 4, organoids were passaged at 1:3 dilution and cultured at 37°C in a standard incubator (humidified, 5% CO_2). Images of organoids were taken using EVOS Cell Imaging System (Thermo Fisher Scientific) with a 20× objective at various time points.

Statistics

All experiments were repeated at least two times. Unless specified, all quantitative data were presented as mean ± SEM. Student's *t* test was used to assess the statistical significance of differences between two groups. One-way ANOVA followed by the Bonferroni post-test was used to analyze the significance of differences among three or more groups. The Fisher's exact test was used to determine the significance of differences in the percentage of incidence among groups. For quantitative analysis of antigen expression in tissue arrays, all statistical analysis was performed by SPSS 20.0 software. The association between Tn or Casp1 expression and the clinicopathological factors was estimated using the Fisher's exact or likelihood ratio χ^2 test. The correlation between Tn and Casp1 expression was analyzed using the McNemar χ^2 test. P value < 0.05 was considered to be significant. Data were plotted and analyzed using GraphPad Prism version 5.0 (GraphPad).

Online supplemental material

Fig. S1 shows gastric disease development beginning in neonatal mice and characterizes spontaneous gastric carcinoma in aged mice. Fig. S2 describes further analysis of gastric pathology in the context of inflammasome deficiency. Fig. S3 shows the effect of Abxs on *Helicobacter* species and further characterization of mucin and trefoil family gene expression and the effect of Abx or genetic intervention on mucin expression. Fig. S4 compares growth of gastric antrum organoids from WT versus GEC *C1galt1*$^{-/-}$ mice and Tn staining patterns before and after proton pump inhibition. Table S1 describes the association between Tn expression and clinicopathological characteristics in human gastric cancer patients. Table S2 describes the association between Casp1 expression and clinicopathological characteristics in human gastric cancer patients. Table S3 shows statistical analysis of IHC staining for Tn and Casp1 in a human gastric cancer tissue microarray. Table S4 describes the relationship between Casp1 p10 expression and clinical characteristics of human gastric cancer patients. Table S5 describes the parameters for histological scoring of gastric disease. Table S6 summarizes the primer sequences for mouse tissue cytokine studies. Table S7 summarizes the primer sequences for bacterial studies.

Acknowledgments

This work is supported by the China Scholarship Council, Jiangsu Provincial Natural Science Foundation (grant SBK2019042420), the Jiangsu Provincial Special Program of Medical Science (grants BL2014046 and BL2012005), the Jiangsu Provincial Key Medical Center (grant YXZXA2016002), the Priority Academic Program Development of Jiangsu Higher Education Institutions, the National Natural Science Foundation of China (grant 81902805), Jiangsu Provincial Natural Science Foundation (grant BK20190174), the Oklahoma Center for Adult Stem Cell Research, and an Oklahoma Medical Research Foundation research grant.

The authors declare no competing financial interests.

Author contributions: J. Fu, W. Chen, and L. Xia conceived of and designed the study; F. Liu, J. Fu, K. Bergstrom, X. Shan, J.M. McDaniel, S McGee, and X. Bai performed the experiments; F. Liu, J. Fu, K. Bergstrom, W. Chen, and L. Xia analyzed the data; and F. Liu, K. Bergstrom, W. Chen, and L. Xia wrote the manuscript.

Submitted: 16 December 2018
Revised: 12 August 2019
Accepted: 17 September 2019

References

Arthur, J.C., E. Perez-Chanona, M. Mühlbauer, S. Tomkovich, J.M. Uronis, T.-J. Fan, B.J. Campbell, T. Abujamel, B. Dogan, A.B. Rogers, et al. 2012. Intestinal inflammation targets cancer-inducing activity of the microbiota. *Science.* 338:120–123. https://doi.org/10.1126/science.1224820

Balmaña, M., S. Mereiter, F. Diniz, T. Feijão, C.C. Barrias, and C.A. Reis. 2018. Multicellular Human Gastric-Cancer Spheroids Mimic the Glycosylation Phenotype of Gastric Carcinomas. *Molecules.* 23:E2815. https://doi.org/10.3390/molecules23112815

Barresi, G., G. Giuffrè, E. Vitarelli, M. Grosso, and G. Tuccari. 2001. The immunoexpression of Tn, sialyl-Tn and T antigens in chronic active gastritis in relation to Helicobacter pylori infection. *Pathology.* 33: 298–302. https://doi.org/10.1080/00313020126324

Bergstrom, K., X. Liu, Y. Zhao, N. Gao, Q. Wu, K. Song, Y. Cui, Y. Li, J.M. McDaniel, S. McGee, et al. 2016. Defective Intestinal Mucin-Type O-Glycosylation Causes Spontaneous Colitis-Associated Cancer in Mice. *Gastroenterology.* 151:152–164.e11. https://doi.org/10.1053/j.gastro.2016.03.039

Bergstrom, K., J. Fu, M.E. Johansson, X. Liu, N. Gao, Q. Wu, J. Song, J.M. McDaniel, S. McGee, W. Chen, et al. 2017. Core 1- and 3-derived O-glycans collectively maintain the colonic mucus barrier and protect against spontaneous colitis in mice. *Mucosal Immunol.* 10:91–103. https://doi.org/10.1038/mi.2016.45

Bhaskar, K.R., D.H. Gong, R. Bansil, S. Pajevic, J.A. Hamilton, B.S. Turner, and J.T. LaMont. 1991. Profound increase in viscosity and aggregation of pig gastric mucin at low pH. *Am. J. Physiol.* 261:G827–G832.

Bhaskar, K.R., P. Garik, B.S. Turner, J.D. Bradley, R. Bansil, H.E. Stanley, and J.T. LaMont. 1992. Viscous fingering of HCl through gastric mucin. *Nature.* 360:458–461. https://doi.org/10.1038/360458a0

Borén, T., P. Falk, K.A. Roth, G. Larson, and S. Normark. 1993. Attachment of Helicobacter pylori to human gastric epithelium mediated by blood group antigens. *Science.* 262:1892–1895. https://doi.org/10.1126/science.8018146

Correa, P. 1992. Human gastric carcinogenesis: a multistep and multifactorial process–First American Cancer Society Award Lecture on Cancer Epidemiology and Prevention. *Cancer Res.* 52:6735–6740.

David, L., J.M. Nesland, H. Clausen, F. Carneiro, and M. Sobrinho-Simoes. 1992. Simple mucin-type carbohydrate antigens (Tn, sialosyl-Tn and T) in gastric mucosa, carcinomas and metastases. *APMIS Suppl.* 27:162–172.

Duarte, H.O., D. Freitas, C. Gomes, J. Gomes, A. Magalhães, and C.A. Reis. 2016. Mucin-Type O-Glycosylation in Gastric Carcinogenesis. *Biomolecules.* 6:E33. https://doi.org/10.3390/biom6030033

Duarte, H.O., M. Balmaña, S. Mereiter, H. Osório, J. Gomes, and C.A. Reis. 2017. Gastric Cancer Cell Glycosylation as a Modulator of the ErbB2 Oncogenic Receptor. *Int. J. Mol. Sci.* 18:E2262. https://doi.org/10.3390/ijms18112262

Feng, S., K. Ku, E. Hodzic, E. Lorenzana, K. Freet, and S.W. Barthold. 2005. Differential detection of five mouse-infecting helicobacter species by multiplex PCR. *Clin. Diagn. Lab. Immunol.* 12:531–536.

Fox, J.G., A.B. Rogers, M.T. Whary, Z. Ge, M. Ohtani, E.K. Jones, and T.C. Wang. 2007. Accelerated progression of gastritis to dysplasia in the pyloric antrum of TFF2 -/- C57BL6 x Sv129 Helicobacter pylori-infected mice. *Am. J. Pathol.* 171:1520–1528. https://doi.org/10.2353/ajpath.2007.070249

Freitas, D., D. Campos, J. Gomes, F. Pinto, J.A. Macedo, R. Matos, S. Mereiter, M.T. Pinto, A. Polónia, F. Gartner, et al. 2019. O-glycans truncation modulates gastric cancer cell signaling and transcription leading to a more aggressive phenotype. *EBioMedicine.* 40:349–362. https://doi.org/10.1016/j.ebiom.2019.01.017

Fu, J., H. Gerhardt, J.M. McDaniel, B. Xia, X. Liu, L. Ivanciu, A. Ny, K. Hermans, R. Silasi-Mansat, S. McGee, et al. 2008. Endothelial cell O-glycan deficiency causes blood/lymphatic misconnections and consequent fatty liver disease in mice. *J. Clin. Invest.* 118:3725–3737. https://doi.org/10.1172/JCI36077

Fu, C., H. Zhao, Y. Wang, H. Cai, Y. Xiao, Y. Zeng, and H. Chen. 2016. Tumor-associated antigens: Tn antigen, sTn antigen, and T antigen. *HLA.* 88:275–286. https://doi.org/10.1111/tan.12900

Gao, N., K. Bergstrom, J. Fu, B. Xie, W. Chen, and L. Xia. 2016. Loss of intestinal O-glycans promotes spontaneous duodenal tumors. *Am. J. Physiol. Gastrointest. Liver Physiol.* 311:G74–G83. https://doi.org/10.1152/ajpgi.00060.2016

Heneghan, M.A., A.P. Moran, K.M. Feeley, E.L. Egan, J. Goulding, C.E. Connolly, and C.F. McCarthy. 1998. Effect of host Lewis and ABO blood group antigen expression on Helicobacter pylori colonisation density and the consequent inflammatory response. *FEMS Immunol. Med. Microbiol.* 20:257–266. https://doi.org/10.1111/j.1574-695X.1998.tb01135.x

Hitzler, I., A. Sayi, E. Kohler, D.B. Engler, K.N. Koch, W.-D. Hardt, and A. Müller. 2012. Caspase-1 has both proinflammatory and regulatory properties in Helicobacter infections, which are differentially mediated by its substrates IL-1β and IL-18. *J. Immunol.* 188:3594–3602. https://doi.org/10.4049/jimmunol.1103212

Hoffmann, W. 2015. TFF2, a MUC6-binding lectin stabilizing the gastric mucus barrier and more (Review). *Int. J. Oncol.* 47:806–816. https://doi.org/10.3892/ijo.2015.3090

Holmén Larsson, J.M., K.A. Thomsson, A.M. Rodríguez-Piñeiro, H. Karlsson, and G.C. Hansson. 2013. Studies of mucus in mouse stomach, small intestine, and colon. III. Gastrointestinal Muc5ac and Muc2 mucin O-glycan patterns reveal a regiospecific distribution. *Am. J. Physiol. Gastrointest. Liver Physiol.* 305:G357–G363. https://doi.org/10.1152/ajpgi.00048.2013

Ilver, D., A. Arnqvist, J. Ogren, I.M. Frick, D. Kersulyte, E.T. Incecik, D.E. Berg, A. Covacci, L. Engstrand, and T. Borén. 1998. Helicobacter pylori adhesin binding fucosylated histo-blood group antigens revealed by retagging. *Science.* 279:373–377. https://doi.org/10.1126/science.279.5349.373

Johansson, M., I. Synnerstad, and L. Holm. 2000. Acid transport through channels in the mucous layer of rat stomach. *Gastroenterology.* 119:1297–1304. https://doi.org/10.1053/gast.2000.19455

Johansson, M.E., H. Sjövall, and G.C. Hansson. 2013. The gastrointestinal mucus system in health and disease. *Nat. Rev. Gastroenterol. Hepatol.* 10:352–361. https://doi.org/10.1038/nrgastro.2013.35

Ju, T., and R.D. Cummings. 2002. A unique molecular chaperone Cosmc required for activity of the mammalian core 1 beta 3-galactosyltransferase. *Proc. Natl. Acad. Sci. USA.* 99:16613–16618. https://doi.org/10.1073/pnas.262438199

Ju, T., R.P. Aryal, C.J. Stowell, and R.D. Cummings. 2008. Regulation of protein O-glycosylation by the endoplasmic reticulum-localized molecular chaperone Cosmc. *J. Cell Biol.* 182:531–542. https://doi.org/10.1083/jcb.200711151

Kameoka, S., T. Kameyama, T. Hayashi, S. Sato, N. Ohnishi, T. Hayashi, N. Murata-Kamiya, H. Higashi, M. Hatakeyama, and A. Takaoka. 2016. Helicobacter pylori induces IL-1β protein through the inflammasome activation in differentiated macrophagic cells. *Biomed. Res.* 37:21–27. https://doi.org/10.2220/biomedres.37.21

Karasawa, F., A. Shiota, Y. Goso, M. Kobayashi, Y. Sato, J. Masumoto, M. Fujiwara, S. Yokosawa, T. Muraki, S. Miyagawa, et al. 2012. Essential role of gastric gland mucin in preventing gastric cancer in mice. *J. Clin. Invest.* 122:923–934. https://doi.org/10.1172/JCI59087

Kawakubo, M., Y. Ito, Y. Okimura, M. Kobayashi, K. Sakura, S. Kasama, M.N. Fukuda, M. Fukuda, T. Katsuyama, and J. Nakayama. 2004. Natural antibiotic function of a human gastric mucin against Helicobacter pylori infection. *Science.* 305:1003–1006. https://doi.org/10.1126/science.1099250

Kayagaki, N., S. Warming, M. Lamkanfi, L. Vande Walle, S. Louie, J. Dong, K. Newton, Y. Qu, J. Liu, S. Heldens, et al. 2011. Non-canonical inflammasome activation targets caspase-11. *Nature.* 479:117–121. https://doi.org/10.1038/nature10558

Koch, K.N., and A. Müller. 2015. Helicobacter pylori activates the TLR2/NLRP3/caspase-1/IL-18 axis to induce regulatory T-cells, establish persistent infection and promote tolerance to allergens. *Gut Microbes.* 6:382–387. https://doi.org/10.1080/19490976.2015.1105427

Lefebvre, O., M.P. Chenard, R. Masson, J. Linares, A. Dierich, M. LeMeur, C. Wendling, C. Tomasetto, P. Chambon, and M.C. Rio. 1996. Gastric mucosa abnormalities and tumorigenesis in mice lacking the pS2 trefoil protein. *Science.* 274:259–262. https://doi.org/10.1126/science.274.5285.259

Li, T., C. Mo, X. Qin, S. Li, Y. Liu, and Z. Liu. 2018. Glycoprofiling of Early Gastric Cancer Using Lectin Microarray Technology. *Clin. Lab.* 64:153–161. https://doi.org/10.7754/Clin.Lab.2017.170814

Lindén, S., J. Mahdavi, C. Semino-Mora, C. Olsen, I. Carlstedt, T. Borén, and A. Dubois. 2008. Role of ABO secretor status in mucosal innate immunity and H. pylori infection. *PLoS Pathog.* 4:e2. https://doi.org/10.1371/journal.ppat.0040002

Lindén, S.K., Y.H. Sheng, A.L. Every, K.M. Miles, E.C. Skoog, T.H. Florin, P. Sutton, and M.A. McGuckin. 2009. MUC1 limits Helicobacter pylori infection both by steric hindrance and by acting as a releasable decoy. *PLoS Pathog.* 5:e1000617. https://doi.org/10.1371/journal.ppat.1000617

Magalhães, A., J. Gomes, M.N. Ismail, S.M. Haslam, N. Mendes, H. Osório, L. David, J. Le Pendu, R. Haas, A. Dell, et al. 2009. Fut2-null mice display an altered glycosylation profile and impaired BabA-mediated Helicobacter pylori adhesion to gastric mucosa. *Glycobiology.* 19:1525–1536. https://doi.org/10.1093/glycob/cwp131

Marshall, B.J. 1995. Helicobacter pylori in peptic ulcer: have Koch's postulates been fulfilled? *Ann. Med.* 27:565–568. https://doi.org/10.3109/07853899509002470

McGuckin, M.A., A.L. Every, C.D. Skene, S.K. Linden, Y.T. Chionh, A. Swierczak, J. McAuley, S. Harbour, M. Kaparakis, R. Ferrero, and P. Sutton. 2007. Muc1 mucin limits both Helicobacter pylori colonization of the murine gastric mucosa and associated gastritis. *Gastroenterology.* 133:1210–1218. https://doi.org/10.1053/j.gastro.2007.07.003

Mereiter, S., K. Polom, C. Williams, A. Polonia, M. Guergova-Kuras, N.G. Karlsson, F. Roviello, A. Magalhães, and C.A. Reis. 2018. The Thomsen-Friedenreich Antigen: A Highly Sensitive and Specific Predictor of Microsatellite Instability in Gastric Cancer. *J. Clin. Med.* 7:E256. https://doi.org/10.3390/jcm7090256

Miyoshi, H., and T.S. Stappenbeck. 2013. In vitro expansion and genetic modification of gastrointestinal stem cells in spheroid culture. *Nat. Protoc.* 8:2471–2482. https://doi.org/10.1038/nprot.2013.153

Ng, G.Z., T.R. Menheniott, A.L. Every, A. Stent, L.M. Judd, Y.T. Chionh, P. Dhar, J.C. Komen, A.S. Giraud, T.C. Wang, et al. 2016. The MUC1 mucin protects against Helicobacter pylori pathogenesis in mice by regulation of the NLRP3 inflammasome. *Gut.* 65:1087–1099. https://doi.org/10.1136/gutjnl-2014-307175

Nishihara, S. 2018. Glycans in stem cell regulation: from Drosophila tissue stem cells to mammalian pluripotent stem cells. *FEBS Lett.* 592:3773–3790. https://doi.org/10.1002/1873-3468.13167

Pachathundikandi, S.K., A. Müller, and S. Backert. 2016. Inflammasome Activation by Helicobacter pylori and Its Implications for Persistence and Immunity. *Curr. Top. Microbiol. Immunol.* 397:117–131.

Persson, N., N. Stuhr-Hansen, C. Risinger, S. Mereiter, A. Polónia, K. Polom, A. Kovács, F. Roviello, C.A. Reis, C. Welinder, et al. 2017. Epitope mapping of a new anti-Tn antibody detecting gastric cancer cells. *Glycobiology.* 27:635–645. https://doi.org/10.1093/glycob/cwx033

Peterson, A.J., T.R. Menheniott, L. O'Connor, A.K. Walduck, J.G. Fox, K. Kawakami, T. Minamoto, E.K. Ong, T.C. Wang, L.M. Judd, and A.S. Giraud. 2010. Helicobacter pylori infection promotes methylation and silencing of trefoil factor 2, leading to gastric tumor development in mice and humans. *Gastroenterology.* 139:2005–2017. https://doi.org/10.1053/j.gastro.2010.08.043

Phillipson, M., C. Atuma, J. Henriksnäs, and L. Holm. 2002. The importance of mucus layers and bicarbonate transport in preservation of gastric juxtamucosal pH. *Am. J. Physiol. Gastrointest. Liver Physiol.* 282:G211–G219. https://doi.org/10.1152/ajpgi.00223.2001

Radhakrishnan, P., S. Dabelsteen, F.B. Madsen, C. Francavilla, K.L. Kopp, C. Steentoft, S.Y. Vakhrushev, J.V. Olsen, L. Hansen, E.P. Bennett, et al. 2014. Immature truncated O-glycophenotype of cancer directly induces oncogenic features. *Proc. Natl. Acad. Sci. USA.* 111:E4066–E4075. https://doi.org/10.1073/pnas.1406619111

Rajamäki, K., T. Nordström, K. Nurmi, K.E. Åkerman, P.T. Kovanen, K. Öörni, and K.K. Eklund. 2013. Extracellular acidosis is a novel danger signal alerting innate immunity via the NLRP3 inflammasome. *J. Biol. Chem.* 288:13410–13419. https://doi.org/10.1074/jbc.M112.426254

Rodgers, A.B. 2012. Histologic scoring of gastritis and gastric cancer in mouse models. *In* Helicobacter Species: Methods and Protocols. Springer-Verlag, New York. 189–203.

Ruchaud-Sparagano, M.H., B.R. Westley, and F.E. May. 2004. The trefoil protein TFF1 is bound to MUC5AC in human gastric mucosa. *Cell. Mol. Life Sci.* 61:1946–1954. https://doi.org/10.1007/s00018-004-4124-x

Saqui-Salces, M., A.C. Tsao, M.G. Gillilland III, and J.L. Merchant. 2017. Weight gain in mice on a high caloric diet and chronically treated with omeprazole depends on sex and genetic background. *Am. J. Physiol. Gastrointest. Liver Physiol.* 312:G15–G23. https://doi.org/10.1152/ajpgi.00211.2016

Schade, C., G. Flemström, and L. Holm. 1994. Hydrogen ion concentration in the mucus layer on top of acid-stimulated and -inhibited rat gastric mucosa. *Gastroenterology*. 107:180–188. https://doi.org/10.1016/0016-5085(94)90075-2

Shaked, H., L.J. Hofseth, A. Chumanevich, A.A. Chumanevich, J. Wang, Y. Wang, K. Taniguchi, M. Guma, S. Shenouda, H. Clevers, et al. 2012. Chronic epithelial NF-κB activation accelerates APC loss and intestinal tumor initiation through iNOS up-regulation. *Proc. Natl. Acad. Sci. USA.* 109:14007–14012. https://doi.org/10.1073/pnas.1211509109

Soutto, M., A. Belkhiri, M.B. Piazuelo, B.G. Schneider, D. Peng, A. Jiang, M.K. Washington, Y. Kokoye, S.E. Crowe, A. Zaika, et al. 2011. Loss of TFF1 is associated with activation of NF-κB-mediated inflammation and gastric neoplasia in mice and humans. *J. Clin. Invest.* 121:1753–1767. https://doi.org/10.1172/JCI43922

Springer, G.F. 1984. T and Tn, general carcinoma autoantigens. *Science.* 224:1198–1206. https://doi.org/10.1126/science.6729450

Sun, X., T. Ju, and R.D. Cummings. 2018. Differential expression of Cosmc, T-synthase and mucins in Tn-positive colorectal cancers. *BMC Cancer.* 18:827. https://doi.org/10.1186/s12885-018-4708-8

Torre, L.A., F. Bray, R.L. Siegel, J. Ferlay, J. Lortet-Tieulent, and A. Jemal. 2015. Global cancer statistics, 2012. *CA Cancer J. Clin.* 65:87–108. https://doi.org/10.3322/caac.21262

Wang, Y., T. Ju, X. Ding, B. Xia, W. Wang, L. Xia, M. He, and R.D. Cummings. 2010. Cosmc is an essential chaperone for correct protein O-glycosylation. *Proc. Natl. Acad. Sci. USA.* 107:9228–9233. https://doi.org/10.1073/pnas.0914004107

Wang, L., H. Fu, G. Nanayakkara, Y. Li, Y. Shao, C. Johnson, J. Cheng, W.Y. Yang, F. Yang, M. Lavallee, et al. 2016. Novel extracellular and nuclear caspase-1 and inflammasomes propagate inflammation and regulate gene expression: a comprehensive database mining study. *J. Hematol. Oncol.* 9:122. https://doi.org/10.1186/s13045-016-0351-5

Werther, J.L., S. Rivera-MacMurray, H. Bruckner, M. Tatematsu, and S.H. Itzkowitz. 1994. Mucin-associated sialosyl-Tn antigen expression in gastric cancer correlates with an adverse outcome. *Br. J. Cancer.* 69:613–616. https://doi.org/10.1038/bjc.1994.114

Yi, J., K. Bergstrom, J. Fu, X. Shan, J.M. McDaniel, S. McGee, D. Qu, C.W. Houchen, X. Liu, and L. Xia. 2019. Dclk1 in tuft cells promotes inflammation-driven epithelial restitution and mitigates chronic colitis. *Cell Death Differ.* 26:1656–1669. https://doi.org/10.1038/s41418-018-0237-x

Yin, S., C. Lan, H. Pei, and Z. Zhu. 2015. Expression of interleukin 1β in gastric cancer tissue and its effects on gastric cancer. *OncoTargets Ther.* 9:31–35. https://doi.org/10.2147/OTT.S94277

Supplemental material

Liu et al., https://doi.org/10.1084/jem.20182325

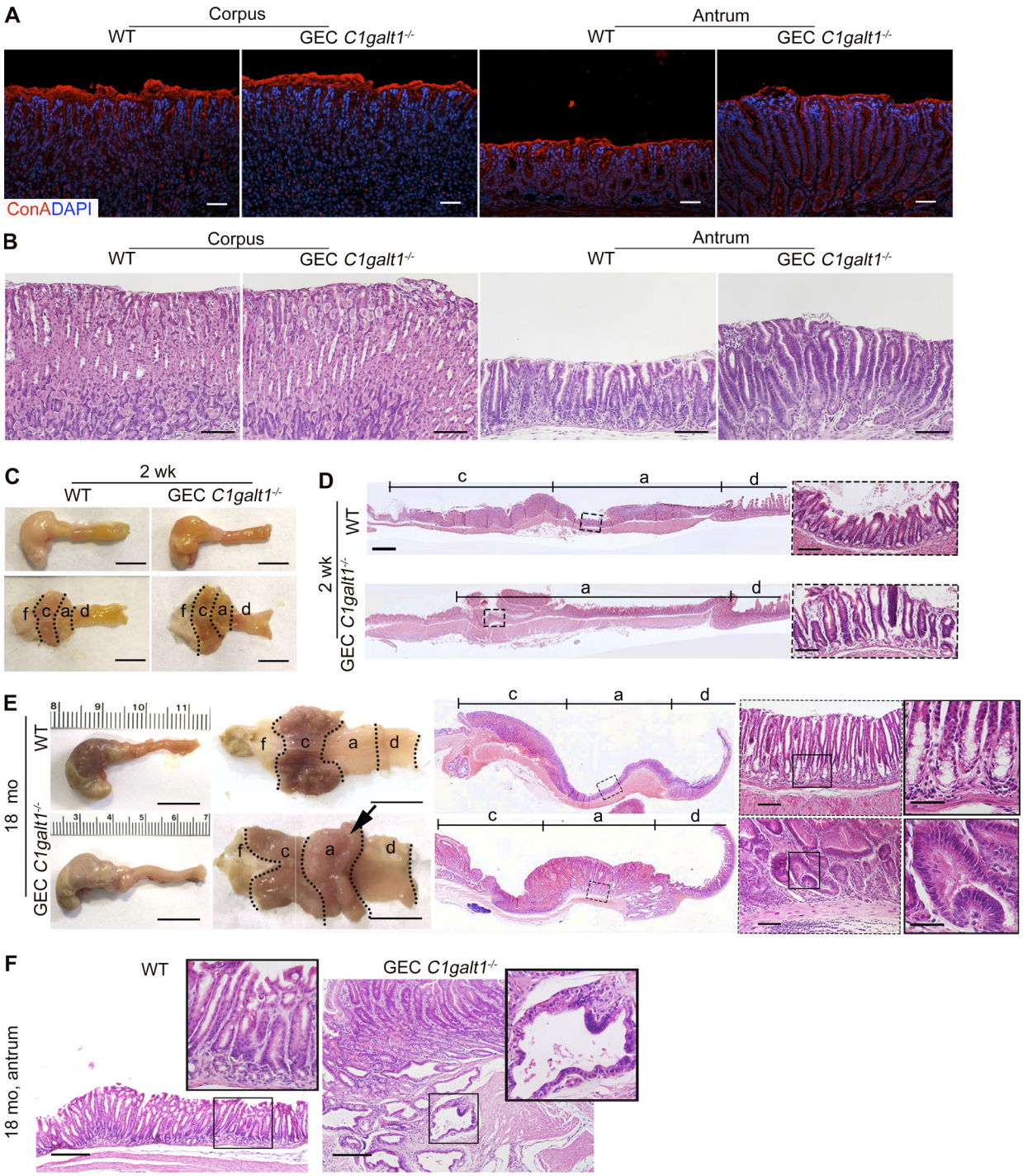

Figure S1. **GEC *C1galt1*$^{-/-}$ mice develop spontaneous gastritis at an early age and gastric cancer at age 18 mo. (A)** Representative images of IF-stained WT and GEC *C1galt1*$^{-/-}$ stomach sections. **(B)** H&E staining of corpus and antrum. **(C)** Representative gross morphology of murine stomach (n = 4–5 mice/group). Scale bars, 1 cm. a, antrum; c, corpus; d, duodenum; f, forestomach. **(D)** H&E staining of stomach sections. Inset: Magnified portion of boxed region in left image. Scale bars, 200 µm (tiling images); 50 µm (inset). **(E)** Representative gross morphology of murine stomach (n = 4–5 mice/group). Arrow shows a large antral tumor. Scale bars, 1 cm (gross morphology); 200 µm (tiling images); 50 µm (left inset); 25 µm (right inset). **(F)** H&E staining of antrum. Inset: Magnified image of boxed region. Scale bars, 100 µm.

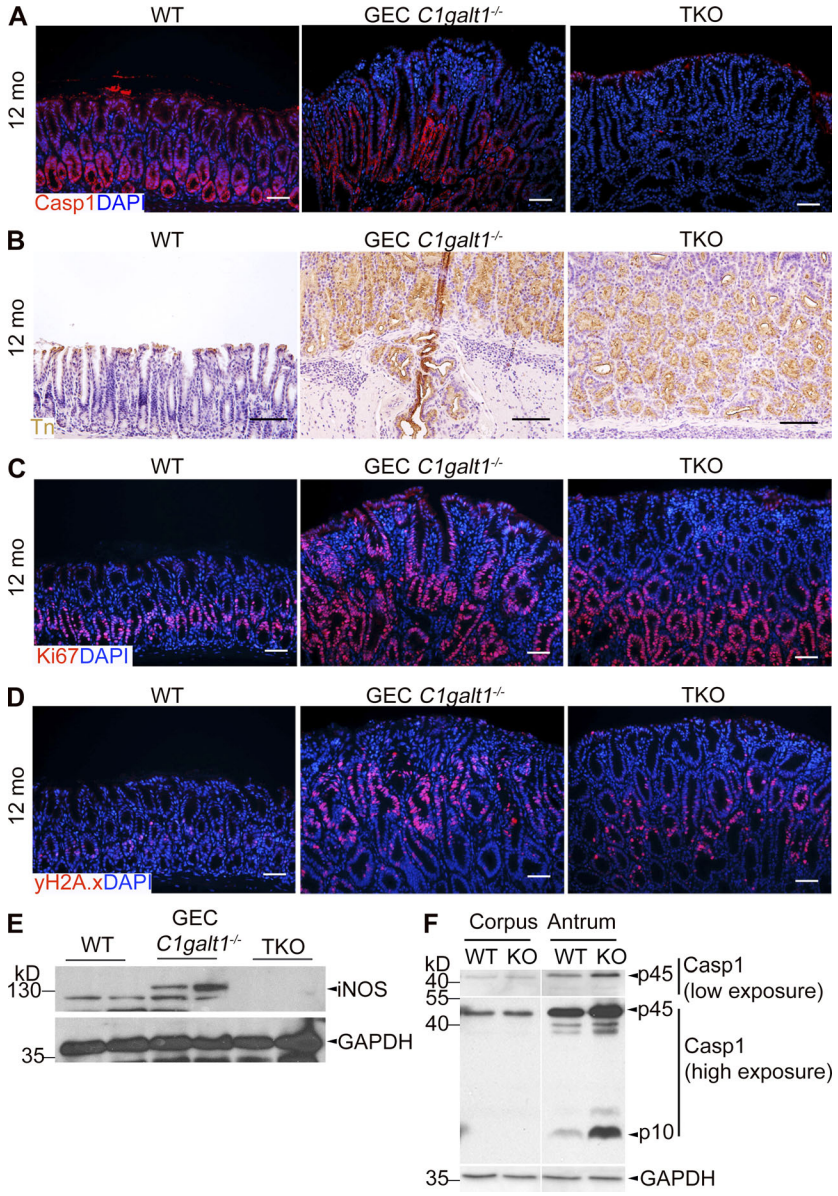

Figure S2. **Characterization of gastric pathology in inflammasome-deficient GEC *C1galt1*$^{-/-}$ mice. (A)** Representative images of IF staining on antrum tissues. **(B)** IHC for Tn antigen (brown). **(C and D)** IF staining for Ki-67 (C) and γ-H2A.X (D). Scale bars, 50 µm. **(E)** Western blot for inducible nitric oxide synthase (iNOS) in gastric antrum tissues. Scale bars, 50 µm. **(F)** Western blot for Casp1 expression and activation status in different stomach regions.

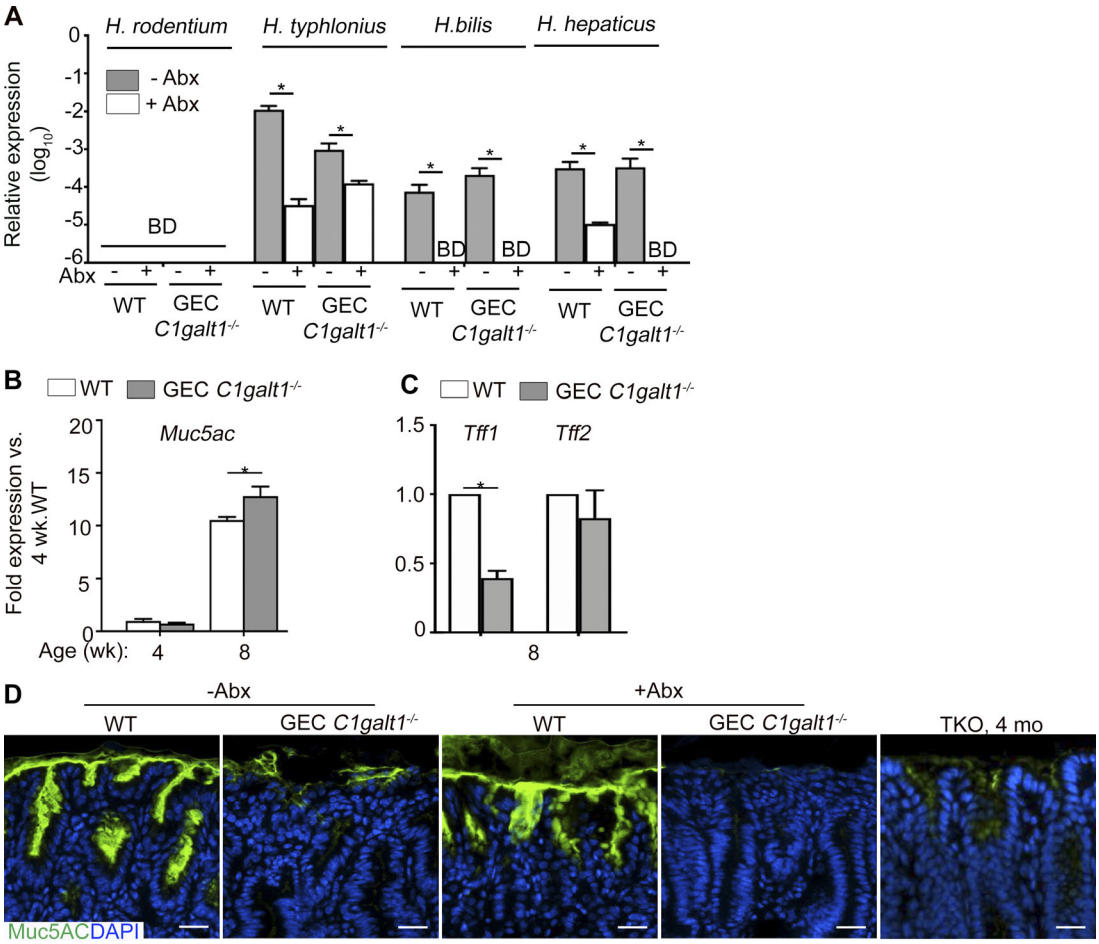

Figure S3. ***Helicobacter* species detection and *muc5ac* and related gene expression in gastric tissues and their relationship to microbiota and inflammation in situ. (A)** qPCR using *Helicobacter* species–specific primers on stomach gDNA. BD, below detection. **(B)** qPCR analysis of gastric antrum tissues at various time points. **(C)** qPCR analysis as in A, but in 8-wk-old mice only. **(D)** IF staining of gastric antrum sections of 8-wk-old mice. Data are representative of four mice per group (mean ± SD). *, P < 0.05.

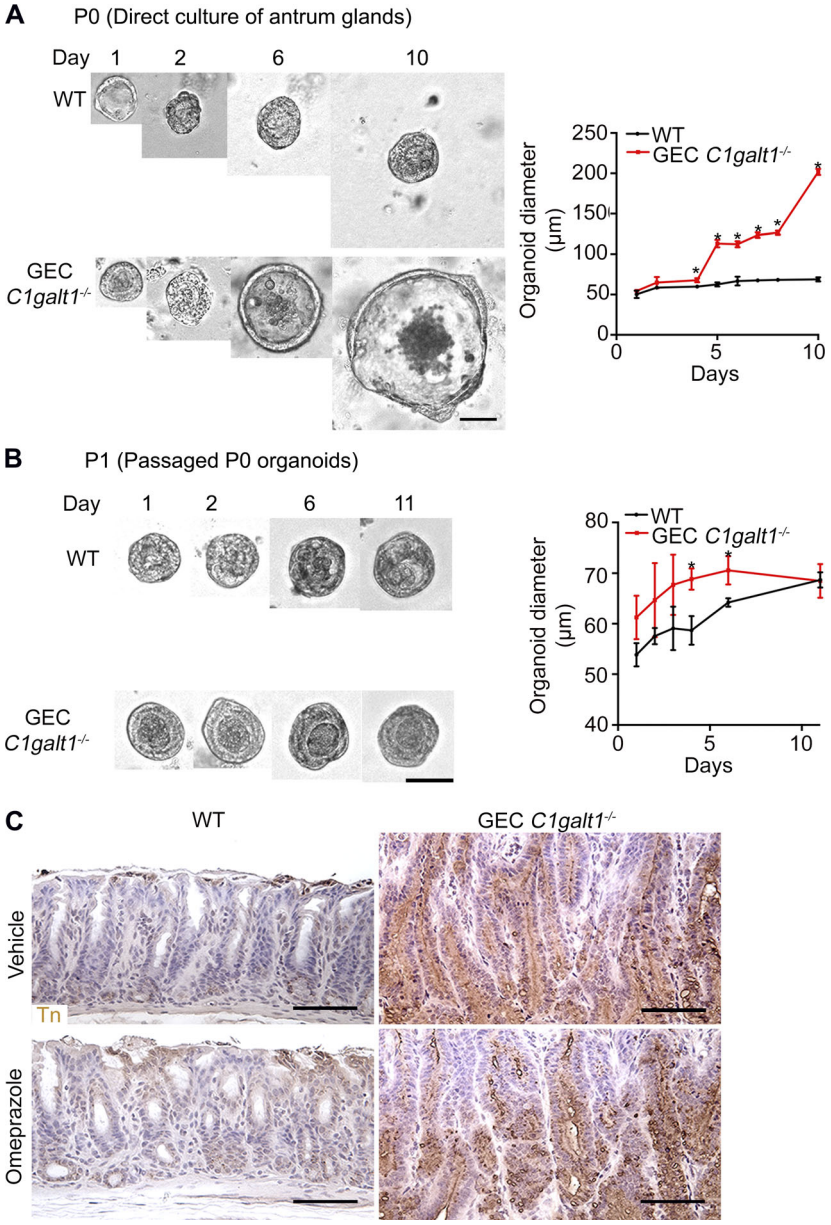

Figure S4. **Effect of C1GalT1 loss on growth of primary antrum epithelial cells. (A)** Representative antrum gland–derived organoids at successive days after culture. Graph shows measurement or gastric spheroid diameter (mean ± SD). *, P < 0.05. **(B)** Same as A, but analyzed after the first passage (P1). Results are representative of two independent experiments (mean ± SD). *, P < 0.05. **(C)** IHC staining of WT and GEC *C1galt1*$^{-/-}$ antrum with anti-Tn. Brown, positive staining. Scale bars, 50 µm.

Table S1. **Association between Tn expression and clinicopathological characteristics in humans**

Characteristics	*n*	Tn expression		P value
		Low (%)	High (%)	
Total	29	6 (20.7)	23 (79.3)	
Gender				
Male	18	3 (16.7)	15 (83.3)	0.646
Female	11	3 (27.3)	8 (72.7)	
Age (yr)				
<60	15	2 (13.3)	13 (86.7)	0.390
≥60	14	4 (28.6)	10 (71.4)	
Histological type				
Adenocarcinoma	16	3 (18.8)	13 (81.2)	0.502
Tubular adenocarcinoma	2	1 (50.0)	1 (50.0)	
Mucinous adenocarcinoma	3	0 (0.0)	3 (100.0)	
Signet ring cell adenocarcinoma	8	2 (25.0)	6 (75.0)	
Tumor diameter				
<5 cm	15	5 (33.3)	10 (66.7)	0.169
≥5 cm	14	1 (7.1)	13 (92.9)	
Tumor location				
Cardia	4	1 (25.0)	3 (75.0)	0.758
Fundus	2	1 (50.0)	1 (50.0)	
Body	6	1 (16.7)	5 (83.3)	
Antrum	15	3 (20.0)	12 (80.0)	
Whole stomach	2	0 (0.0)	2 (100.0)	
Degree of inflammation				
Low	5	3 (60.0)	2 (40.0)	0.046
High	24	3 (12.5)	21 (87.5)	
***H. pylori* infection status**				
Yes	23	3 (13.0)	20 (87.0)	0.083
No	6	3 (50.0)	3 (50.0)	
Tumor differentiation				
Well/moderately	12	4 (33.3)	8 (66.7)	0.198
Poorly	17	2 (11.8)	15 (88.2)	
TNM stage				
I or II	14	6 (42.9)	8 (57.1)	0.006
III or IV	15	0 (0.0)	15 (100.0)	

Table S2. **Association between Casp1 expression and clinicopathological characteristics in human gastric cancer patients**

Characteristics	*n*	Casp1 expression		P value
		Low (%)	High (%)	
Total	29	12 (41.4)	17 (58.6)	
Gender				
Male	18	7 (38.9)	11 (61.1)	1.000
Female	11	5 (45.5)	6 (54.5)	
Age (yr)				
<65	15	8 (53.3)	7 (46.7)	0.264
≥65	14	4 (28.6)	10 (71.4)	
Histological type				
Adenocarcinoma	16	6 (37.5)	10 (62.5)	0.804
Tubular adenocarcinoma	2	1 (50.0)	1 (50.0)	
Mucinous adenocarcinoma	3	2 (66.7)	1 (33.3)	
Signet ring cell adenocarcinoma	8	3 (37.5)	5 (62.5)	
Tumor diameter				
<5 cm	15	7 (46.7)	8 (53.3)	0.710
≥5 cm	14	5 (35.7)	9 (64.3)	
Tumor location				
Cardia	4	1 (25.0)	3 (75.0)	0.941
Fundus	2	1 (50.0)	1 (50.0)	
Body	6	3 (50.0)	3 (50.0)	
Antrum	15	6 (40.0)	9 (60.0)	
Whole stomach	2	1 (50.0)	1 (50.0)	
Degree of inflammation				
Low	5	5 (100.0)	0 (0.0)	0.007
High	24	7 (29.2)	17 (70.8)	
***H. pylori* infection status**				
Yes	23	7 (30.4)	16 (69.6)	0.056
No	6	5 (83.3)	1 (16.7)	
Tumor differentiation				
Well/moderately	12	8 (66.7)	4 (33.3)	0.029
Poorly	17	4 (23.5)	13 (76.5)	
TNM stage				
I or II	14	9 (64.3)	5 (35.7)	0.025
III or IV	15	3 (20.0)	12 (80.0)	

Table S3. **Statistical analysis of IHC staining for Tn and Casp1 in a human gastric cancer tissue microarray**

	Tn expression		
Casp1 expression	**Low (%)**	**High (%)**	**Total**
Low (%)	6 (50.0)	6 (50.0)	12
High (%)	0 (0.0)	17 (100.0)	17
Total	6	23	29

P = 0.031.

Table S4. **Relationship between Casp1 p10 expression and clinical characteristics of human gastric cancer patients**

Characteristics	No. of patients (total = 30)	Casp1 p10 expression		P value
		Negative (*n* = 11)	Positive (*n* = 19)	
Age (yr)				
<65	12	6	6	0.266
≥65	18	5	13	
Gender				
Male	15	3	12	0.128
Female	15	8	7	
Histological type				
Adenocarcinoma	18	7	11	0.955
Tubular adenocarcinoma	5	2	3	
Mucinous adenocarcinoma	3	1	2	
Signet ring cell adenocarcinoma	4	1	3	
Tumor diameter				
<5 cm	16	5	11	0.707
≥5 cm	14	6	8	
Tumor location				
Cardia	6	2	4	0.787
Fundus	2	1	1	
Body	5	3	2	
Antrum	14	4	10	
Whole stomach	3	1	2	
Degree of inflammation				
Low	6	5	1	0.016
High	24	6	18	
***H. pylori* infection status**				
Yes	25	7	18	0.047
No	5	4	1	
Tumor differentiation				
Well/moderately	13	3	10	0.259
Poorly	17	8	9	
TNM stage				
I or II	11	7	4	0.047
III or IV	19	4	15	

Table S5. **Parameters for histological scoring of gastric disease**

Parameter	1	2	3	4
Inflammation	Multifocal aggregates of mononuclear ± polymorphonuclear leukocytes (arrows)	Coalescing aggregates of inflammatory cells in submucosa ± mucosa (mononuclear predominat)	Organizing nodules of lymphocytes and other inflammatory cells in submucosa ± mucosa	Follicles and/or sheets of inflammatory cells extending into or through muscularis ± adventitia
Epithelial defects	Tattered epithelial surface; occasional dilated glands with sloughed apoptotic cells	Distinctly attenuated surface epithelium; numerous ectatic glands and necrotic cells and debris	Inapparent surface epithelial lining; few if any recognizable gastric pits	Mucosal erosions with multifocal collapse and fibrosis; surface lined by fibrin and/or inflammatory cell debris
Hyperplasia	Moderate elongation of gastric pits	Surface-type epithelium increased at least two times the normal length; some loss of oxyntic glands	Three times or more elongation of surface-type epithelium with significant loss of zymogenic glands	Four times or more elongation of surface-type or dysplastic epithelium; complete loss of function mucosa
Dysplasia	Multifocal dysplastic glands characterized by elongation, altered shapes, back-to-back forms, etc.	Coalescing dysplasia with glandular ectasia, branching, infolding, cell piling up, globoid cells, etc.	Gastric intraepithelial neoplasia; loss of normal architecture and columnar orientation; atypical hyperchromatic cells	Invasive adenocarcinoma extending into submucosa, vessels, lymphatics, and/or deeper layers

Adapted from Rogers, A.B. Histological scoring of gastritis and gastric cancer in mouse models. *In Helicobacter* Species: Methods and Protocols, Methods in Molecular Biology, vol. 921. J. Houghton, ed. Humana Press, Totowa, New Jersey. Table S4 is reprinted with permission from Humana Press.

Table S6. **Primers for cytokine analysis**

Gene	Forward primer (5′ to 3′)	Reverse primer (5′ to 3′)
il6	GAGGATACCACTCCCAACAGACC	AAGTGCATCATCGTTGTTCAT
il17a	TCAAAGCTCAGCGTGTCCAA	TCTTCATTGCGGTGGAGAGTC
tnf	CATCTTCTCAAAATTCGAGTGACAA	TGGGAGTAGACAAGGTACAACCC
cxcl1	AACCGAAGTCATAGCCACAC	GTTGGATTTGTCACTGTTCAGC
muc5ac	TGGTTTGACACTGACTTCCC	TCCTCTCGGTGACAGAGTCT
tff1	CAAGGTGATCTGTGTCCTGC	CATGATACATGTTTCCTGGG
tff2	CTGACACCCCACAACAGAAA	TCCGATTCTTGGTTTGGAAGT
hprt1	TCGTGATTAGCGATGATGAA	AGTCTTTCAGTCCTGTCCAT

Table S7. **Primers for bacterial analysis**

Gene	Forward primer (5′ to 3′)	Reverse primer (5′ to 3′)
16s	CCATGAAGTCGGAATCGCTAG	ACTCCCATGGTGTGACGG
Helicobacter genus	TATGACGGGTATCCGGC	ATTCCACCTACCTCTCCA
Helicobacter rodentium	TTGTGAAATGGAGCAAATCTTAAAAACT	TTGTGAAATGGAGCAAATCTTAAAAACT
Helicobacter typhlonius	TTGTGAAATGGAGCAAATCTTAAAAACT	TTGTGAAATGGAGCAAATCTTAAAAACT
Helicobacter bilis	TTGTGAAATGGAGCAAATCTTAAAAACT	CTATGCAAGTTGTGCGTTAAGCAT
Helicobacter hepaticus	TTGTGAAATGGAGCAAATCTTAAAAACT	TTGTGAAATGGAGCAAATCTTAAAAACT